Wang and Zhang
Surface Science and Technology (2023) 1:9
https://doi.org/10.1007/s44251-023-00009-2

Surface Science and Technology

REVIEW

Open Access

Interfacial catalysis of metal-oxide nanocatalysts in CO_2 hydrogenation to value-added C1 chemicals

Ziwei Wang[1] and Zhenhua Zhang[1*]

Abstract

Catalytic CO_2 hydrogenation to valuable chemicals is an excellent approach to address the increasingly serious "greenhouse effect" caused by CO_2 emission generated from the utilizations of nonrenewable fossil energies, while such a process is limited by chemical inertia and thermal stability of the CO_2 molecule and complex hydrogenation routes. In this review, we first summarized the recent progresses of metal-oxide nanocatalysts considered as a category of the most promising catalysts in CO_2 hydrogenation to value-added C1 chemicals including CH_4/CO, formic acid/formate, and methanol. These studies involve with different structural factors affecting the metal-oxide interfacial catalysis including the structures of both the metals (type, particle size, morphology/crystal plane, and bimetal alloy) and the supports (type, particle size, crystal phase, morphology/crystal plane, and composite) and their (strong) metal-support interactions so as to identify the key factor determining the reaction activity, product selectivity, and catalytic stability in CO_2 hydrogenation. Finally, we further discuss challenging coupling with future research opportunities for tunable interfacial catalysis of metal-oxide nanocatalysts in CO_2 conversion.

Keywords Interfacial catalysis, Metal-oxide nanocatalysts, CO_2 hydrogenation, CH4/CO, Formic acid/formate, Methanol

1 Introduction

Since the industrial revolution in the eighteenth century, the increasing human activities in the utilization of fossil fuels (coal, oil, and natural gas) have been gradually breaking the balance of the carbon cycle in nature, leading to a dramatic increase of the CO_2 concentration in the atmosphere from ~ 280 ppm before the industrial revolution, to above 400 ppm today, and predicted to be ~ 570 ppm by the end of this century [1, 2]. The increasing amount of CO_2 emission as one of the major components of greenhouse gases impacts negatively on global temperature, climate change, and ocean acidification [3, 4]. Considering these, the leading countries in CO_2 emission have pledged to reduce CO_2 concentration in the atmosphere in the near future, including ours, which has set goals of "Carbon peak" in 2030 and "Carbon neutrality" in 2060. To address so, reducing anthropogenic CO_2 emission is the optimal approach, nonetheless, it is still difficult to realize this idea due to increasing human demands for energy from utilization of fossil fuels.

Taking CO_2 as the feedstock reacting with green hydrogen (H_2) to produce value-added chemicals such as formic acid (FA), alcohols, and hydrocarbons is considered as a more efficient route to cope with this issue [1, 2, 5–10], while this process proceeds very slowly due to highly chemical inertia of CO_2 though it is reachable in view of thermodynamical point. Catalytic CO_2 hydrogenation can (selectively) accelerate the reaction to reach the equilibrium without structural changes

*Correspondence:
Zhenhua Zhang
zhangzh@sxicc.ac.cn
[1] State Key Laboratory of Coal Conversion, Institute of Coal Chemistry, Chinese Academy of Sciences, Taiyuan 030001, People's Republic of China

of the catalysts. The core of a catalytic reaction is the catalyst, thus, choosing suitable catalysts for efficient CO_2 conversion is crucial. Nowadays, there are mainly two categories of heterogeneous catalysts in this reaction reported in literature, respectively are zeolite-based catalysts [11, 12] and oxide-based catalysts [13, 14]. In terms of a diversity of redox and acid–base properties, the oxide-based catalysts have been widely used to exhibit excellent performance in CO_2 hydrogenation [13–16]. For instance, ZnO has been demonstrated as a superb support to use in commercial CO_2-containing syngas to methanol process back to 1960s [15].

As the most typical category in oxide-based catalysts, the metal-oxide nanocatalysts have been frequently used in CO_2 hydrogenation [17–20]. It has been widely recognized that the catalysis of metal-oxide nanocatalysts arises from the synergetic effect of metal-oxide interfaces [13, 21–25], whose structures are determined by the nature of both the metals and the oxides, and their metal-oxide interactions [24, 26–28]. As known to us, catalytic CO_2 hydrogenation to desirable products is challenging because of chemical inertia and thermal stability of the CO_2 molecule with a high C=O bond energy of 806 kJ mol^{-1} and a π_3^4 bond, and complex catalytic hydrogenation routes [29]. Therefore, tailoring the interfacial structures of metal-oxide nanocatalysts by smart designs are contributive to accurate the identification of catalytic active sites and fundamental understanding of catalysis mechanism, consequently, guiding the catalyst design for CO_2 hydrogenation to desirable products.

In this review, we devote to summarizing present studies of the interfacial catalysis of metal-oxide nanocatalysts in CO_2 hydrogenation to value-added C1 chemicals including CH_4/CO, FA/formate, and methanol. The purpose of this work is not to recollect relevant literature regarding the interfacial catalysis of metal-oxide nanocatalysts in CO_2 hydrogenation but rather to explore the factors (types, particle sizes, bimetal, crystal phase, morphology/crystal plane, composites etc.) affecting the interfacial structures and subsequently their interfacial catalysis in CO_2 hydrogenation so as to unveil the key factors determining the activity and selectivity for CO_2 conversion (Fig. 1). This review is organized as follows: a review of the interfacial catalysis in CO_2 hydrogenation to CH_4/CO via an atmospheric reaction (Section 2), FA/formate via a high-pressure batch reaction (Section 3), methanol via a high-pressure flow reaction (Section 4), and ending with a summary and outlook where future opportunities and challenges in elucidating the interfacial catalysis for guiding the catalyst design in CO_2 hydrogenation are outlined.

2 Methane / Carbon monoxide

As one of the typical conversion processes of inert CO_2 to value-added C1 chemicals [30–33], CO_2 hydrogenation under atmospheric pressure can generate two competitive products of CH_4 and CO, respectively arising from the Sabatier reaction (Eq. 1) and the reverse water–gas shift reaction (RWGS, Eq. 2). Such a process is of importance for the sustainable development of human society with many potential commercial applications [34–36]. For instance, the renewable CH_4 gas from CO_2 hydrogenation could be utilized in the existing natural gas infrastructure to replace the underground natural gas sources, as well as efficiently used in the fuel cell and ammonia synthesis industry to remove trace CO from H_2-rich atmosphere to avoid catalyst poisoning [35, 37], while the CO is valuable as one of the feed gases in the Fischer–Tropsch synthesis to produce CH_3OH or long-chain hydrocarbons [38, 39]. Thermodynamically, CO_2 hydrogenation to CH_4 is an exothermic reaction (Eq. 1, ΔH_{298K} = -165 kJ mol^{-1}) and thus highly favored at low

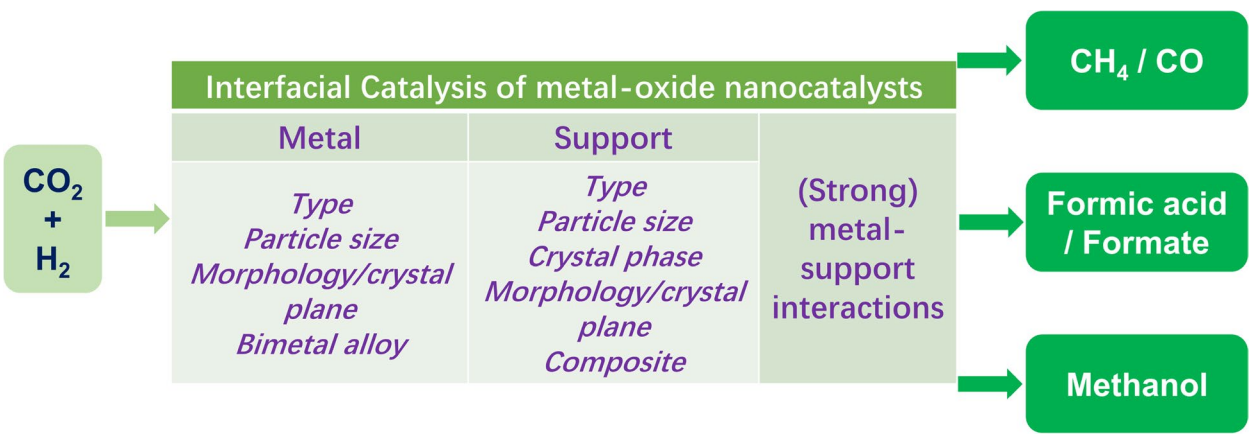

Fig. 1 The theme of this review

temperature. On the contrary, the competitive RWGS reaction is endothermal (Eq. 2, $\Delta H_{298K}=41.2$ kJ mol^{-1}) and normally generates CO at elevated reaction temperatures [40]. A significant challenge in this reaction is to tune the selectivity towards desirable products with a high conversion efficiency due to high chemical inertness of CO_2 molecule and competitive reaction pathways of CO_2 hydrogenation [13].

$$CO_2 + 4H_2 \leftrightarrow CH_4 + 2H_2O\left(\Delta H_{298K} = -165 \text{ kJ mol}^{-1}\right) \quad (1)$$

$$CO_2 + H_2 \leftrightarrow CO + H_2O(\Delta H_{298K} = 41.2 \text{ kJ mol}^{-1}) \quad (2)$$

It has been extensively validated that oxide-supported metal catalysts exhibit excellent performance in this reaction and have drawn considerable attentions [41–43]. Previous studies revealed that the catalytic performance of oxide-supported metal catalysts in CO_2 hydrogenation is sensitive to the metal-oxide interfaces whose structures are determined by both the oxide supports and the supported metals, and their metal-support interactions (MSIs) [13, 23, 24, 44, 45]. Over the past decade, different factors, including the type [23, 46–50], the particle size [24, 26, 51–57], and the bimetal alloying degree [58–65] of supported metals, and the type [21, 46, 66–72], the morphology/crystal plane [23, 24, 73–80], and the composite [72, 81–88] of the supports, as well as the (strong) MSIs [23, 28, 89–96], have been comprehensively investigated to elucidate the interfacial catalysis of oxide-supported metal catalysts in this reaction. In this section, we will focus on the discussions of these structural factors in affecting the interfacial properties and thus the catalytic performance, in order to unveil the key factors determining the activity and selectivity of CO_2 hydrogenation catalyzed by oxide-supported metal catalysts.

2.1 The nature of supported metals

Supported metal nanoparticles (NPs) play crucial roles in CO_2 hydrogenation, which not only serve as the active sites for H_2 activation, but also act as adsorption sites of CO intermediate to contribute to the generation of CH_4 [23, 24, 57]. Consequently, the catalytic performance is strongly dependent on the nature of supported metals [46–65]. Apparently, the type of supported metals directly determines their properties. The commonly-used metals in CO_2 hydrogenation contain Ni, Ru, Rh, Co, and Pd etc., where the inherent nature of metals determines the H_2 dissociation and hydrogenation performance [23, 46–50]. For instance, Quindimil et al. [47] reported that 4%Ru/Al_2O_3 catalyst was quite more active than 12%Ni/Al_2O_3 in CO_2 hydrogenation, which is probably due to the H_2 dissociation capacity greater on the Ru sites. Similarly, Panagiotopoulou's group [48] compared the catalytic performance of different metals supported on TiO_2 in CO_2 hydrogenation and found the turnover frequencies (TOFs) follow an order of Rh > Ru > Pt > Pd (Fig. 2a). Moreover, the CH_4 productions over supported Rh and Ru catalysts are significantly higher than those over supported Pt and Pd catalysts (Fig. 2b), which is mainly ascribed to stronger CO adsorption capacities for the former two to facilitate the reaction of adsorbed CO species with hydrogen atoms to produce CH_4. Our group also compared two commonly-used metals (Ru and Ni) supported on ZnO for CO_2 hydrogenation [23]. Solid experimental evidences confirm the product selectivity is determined by the binding strength of adsorbed CO species on metal sites. A weak CO adsorption capacity on Ni sites contributes to high CO selectivity on all Ni/ZnO catalysts (Fig. 2c1 and c2), while CH_4 is preferentially produced on Ru/ZnO catalysts with stronger CO binding capacity on low-coordination Ru sites (Fig. 2d1 and d2). As a result, Ru/p-ZnO catalyst possessing more amount of low-coordination Ru species induced by stronger Ru-ZnO interactions contributes to higher CH_4 selectivity (Fig. 2d2).

Besides the types, another key factor affecting the interfacial catalysis is the particle size of supported metals, which strongly varies the geometric and electronic structures and thus largely affects their catalytic behaviors [24, 26, 51–57]. This phenomenon has been frequently observed over supported Ni catalysts [52–54, 56, 57]. Hao et al. [52] reported that the CO_2 conversion efficiency decreases with increased Ni particle size from 8 to 21 nm, which could be related to the Ni-CeO_2 interactions and the available surface oxygen vacancies that promote the CO_2 activation. Adversely, the results reported by Lin et al. [53] revealed the catalytic performance catalyzed by Ni/CeO_2 catalysts increase with the Ni particle size growing from 2 to 8 nm, which is demonstrated to be associated with the enhanced hydrogenation property over larger Ni particles. Similar results were also observed by ours [57]. In our previous study, via finely altering the particle size of supported Ni species on CeO_2 from nearly-atomic dispersion to large NPs (Fig. 3a-c), a series of Ni/CeO_2 catalysts were prepared and subsequently used for CO_2 hydrogenation. The results reveal that both the catalytic activity and the CH_4 selectivity increase with the Ni particle size growing up (Fig. 3d and e). With the increased Ni loading accompanied by increased Ni particle size, more interfacial oxygen vacancies probed by a combination of XPS and Raman spectra are responsible for the adsorption and activation of CO_2 that is regarded as the key step for CO_2 hydrogenation, beneficial for the reaction activity; Moreover, the increased mentality of supported Ni species is not only in favor of the H_2 dissociation and hydrogenation properties, but also greatly enhances the CO binding capacity, jointly contributing to the generation of CH_4.

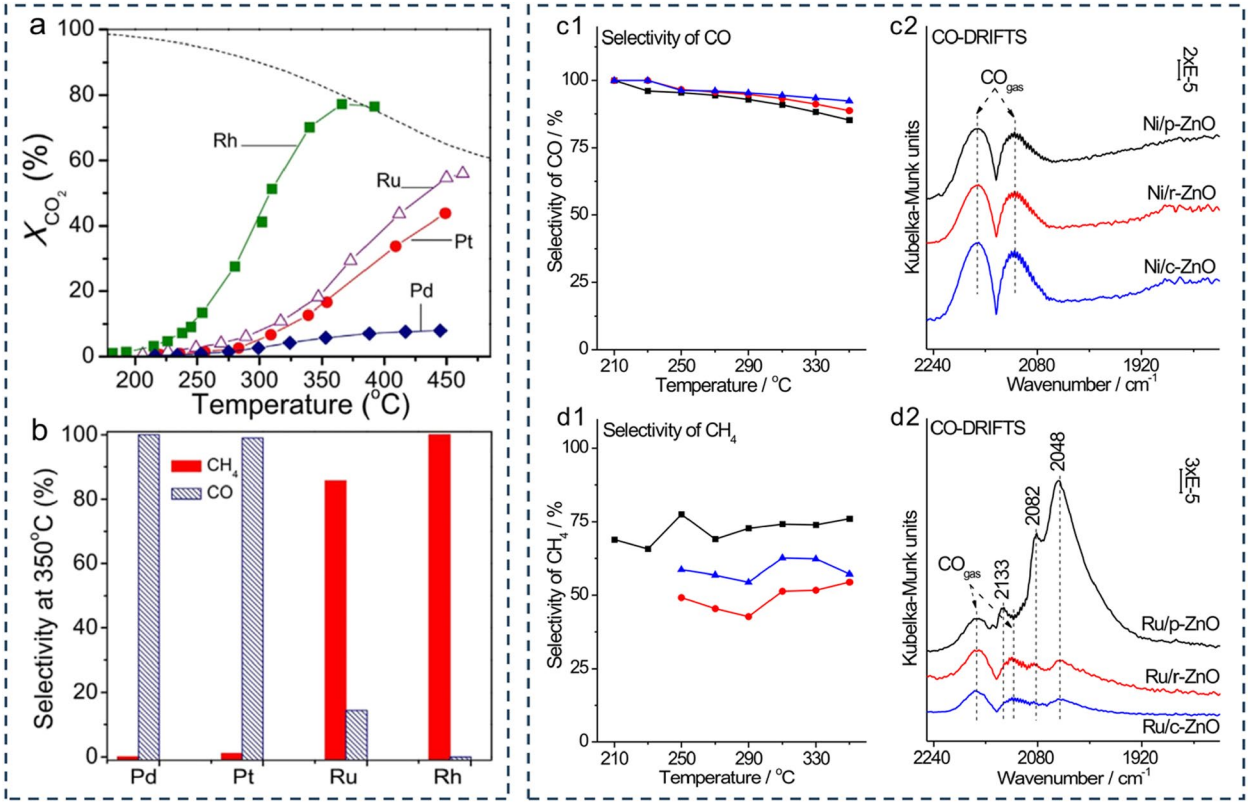

Fig. 2 (a) CO_2 conversions as a function of reaction temperatures and (b) product selectivity at 350 °C obtained over Rh, Ru, Pt and Pd catalysts (0.5 wt.%) supported on TiO_2. (c1, c2) CO selectivity and in situ CO-DRIFTS spectra of different Ni/ZnO catalysts. (d1, d2) CH_4 selectivity and in situ CO-DRIFTS spectra of different Ru/ZnO catalysts. Reprinted with permission from Refs. [23] and [48], Copyright 2022 and 2017, Elsevier

The introduction of an additional metal into the catalyst system can efficiently contribute to reaction activity and stability, and tunable selectivity, which mostly arise from the modified electronic properties and dispersions of active sites via the formation of bimetal alloys [58–65]. Typically, Guo et al. [58] reported that the increased percentage of In atoms in In-Ni intermetallic compounds can facilitate the CO production from CO_2 hydrogenation via the RWGS reaction (Fig. 4a), which could be ascribed to the inhibited CO adsorption at increased In/Ni ratio by isolating the active site of Ni species. In addition to the activity, the formation of bimetal alloy can also promote the product selectivity. The results reported by Wang et al. [59] found that the atomically-dispersed Zn species can stabilize a higher valence state of Ni ($Ni^{\delta+}$) over $NiZn/ZrO_2$ catalysts, leading to the product selectivity in CO_2 hydrogenation shifting from CH_4 to CO (Fig. 4b). Furthermore, the enhanced stability was also realized after introducing an additional metal. Mutz et al. [60] revealed that, compared to commercial Ni-based methanation catalyst, an improved activity and most notably a high stability were observed over Ni_3Fe catalyst (Fig. 4c). Kinetic measurements demonstrate the superior performance for Ni_3Fe catalyst arising from the intimately synergetic effect between Ni and Fe. These results clearly demonstrate the interfacial catalysis of oxide-supported metal catalysts in CO_2 hydrogenation is strongly dependent on the nature of supported metals.

2.2 The nature of the oxide supports

The support plays a crucial role in CO_2 hydrogenation by assisting the dispersion of the active sites, and promoting the activity, selectivity and stability [66–88]. Generally, there are mainly three aspects of the support in affecting the catalyst properties: (1) improving the dispersion of the active sites; (2) weakening the fabrication of the inactive phases; and (3) modifying the reducibility by tuning the active phase-support interactions. Metal oxides have been widely used as catalyst support in CO_2 hydrogenation on basis of their unique redox and acid–base properties [13, 14]. The commonly-used oxides contain ZnO, ZrO_2, CeO_2, Al_2O_3, Y_2O_3, and TiO_2, among which CeO_2 is regarded as a superior catalyst support in CO_2 hydrogenation [21, 46, 66–72]. Díez-Ramírez et al. [66] compared the catalytic performance of different oxides supported Co catalysts in CO_2 hydrogenation and found that the

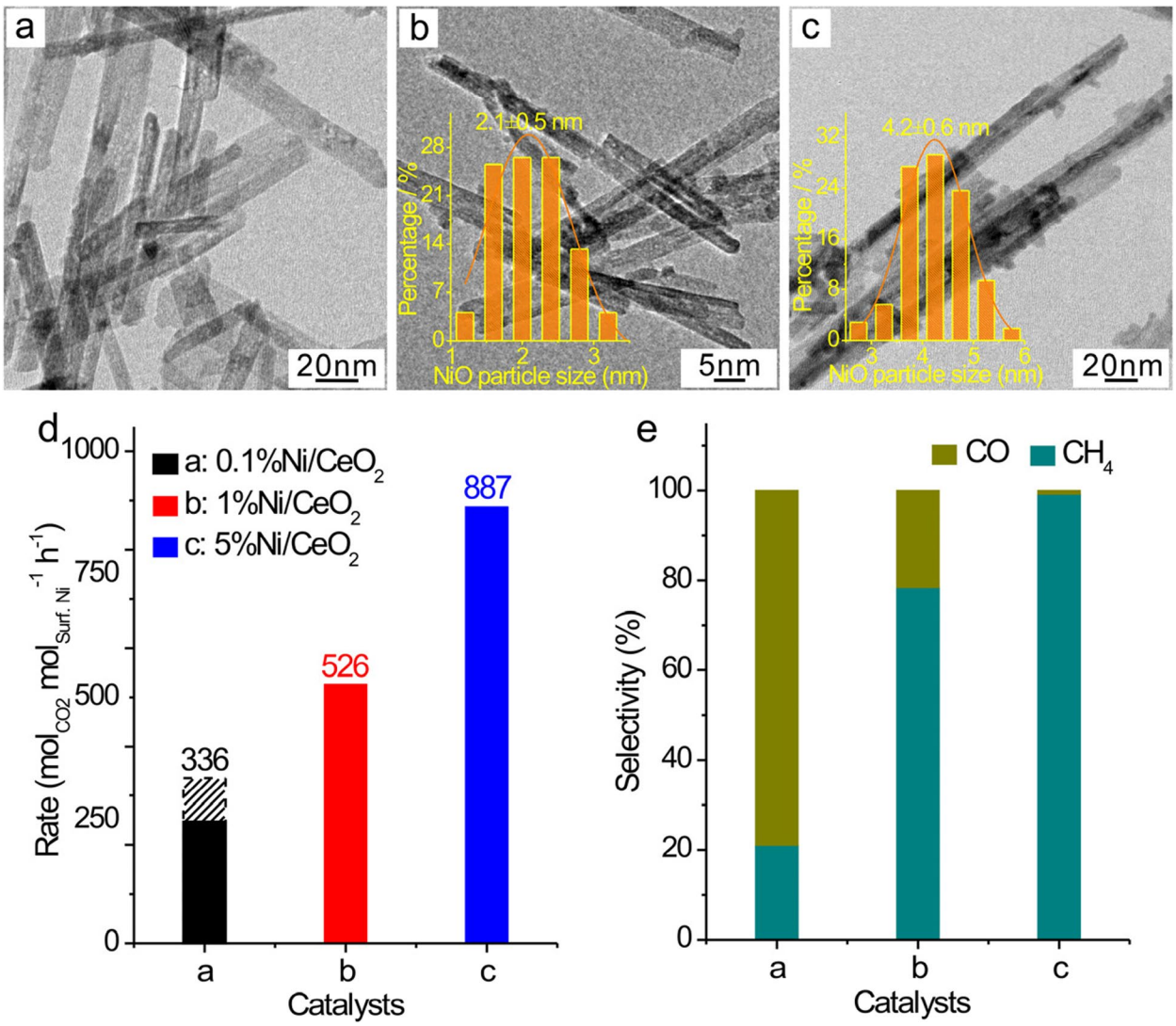

Fig. 3 (a-c) Representative TEM images with corresponding size distributions of NiO nanoparticles. (d) Catalytic activity and (e) product selectivity of CO_2 hydrogenation over various Ni/CeO_2 catalysts at 290 °C. Reprinted with permission from Ref. [57], Copyright 2022, American Chemical Society

catalytic performance in terms of CH_4 yield follows an order of $Co/CeO_2 > Co/ZnO > Co/G_2O_3 > Co/ZrO_2$. Spectroscopic results demonstrate that the superior catalytic performance over Co/CeO_2 catalyst could be ascribed to the enhanced reducibility that is related to the Co-CeO_2 interactions. A large number of studies show that the oxygen vacancies in CeO_2 surface are pivotal in CO_2 hydrogenation, generally responsible for the activation of CO_2 [67, 70, 72]. A typical example was reported by Tada et al. [67], who demonstrate a higher catalytic performance over Ni/CeO_2 catalyst than over Ni/α-Al_2O_3 and Ni/TiO_2 catalysts in CO_2 hydrogenation (Fig. 5a). This is mainly ascribed to higher surface oxygen vacancy concentrations over CeO_2 support that is beneficial for the adsorption and activation of CO_2 and thus the CO_2 conversion. Moreover, Wang et al. [72] found that the surface oxygen vacancies in CeO_2 not only contribute to a much lower activation temperature, but also determine the reaction mechanism (Fig. 5b). In their study, two types of oxides (CeO_2 with surface oxygen vacancies and α-Al_2O_3 without surface oxygen vacancies) were used as supported to load Ru for CO_2 hydrogenation. Operando spectroscopy characterizations demonstrate that the CO_2 hydrogenation catalyzed by Ru/CeO_2 catalyst undergoes a formate route to produce CH_4, in which the formate dissociation to methanol over surface oxygen vacancies is the rate-determining step (RDS). On the contrary, a CO reaction route emerges over Ru/α-Al_2O_3 catalyst due to the absence of

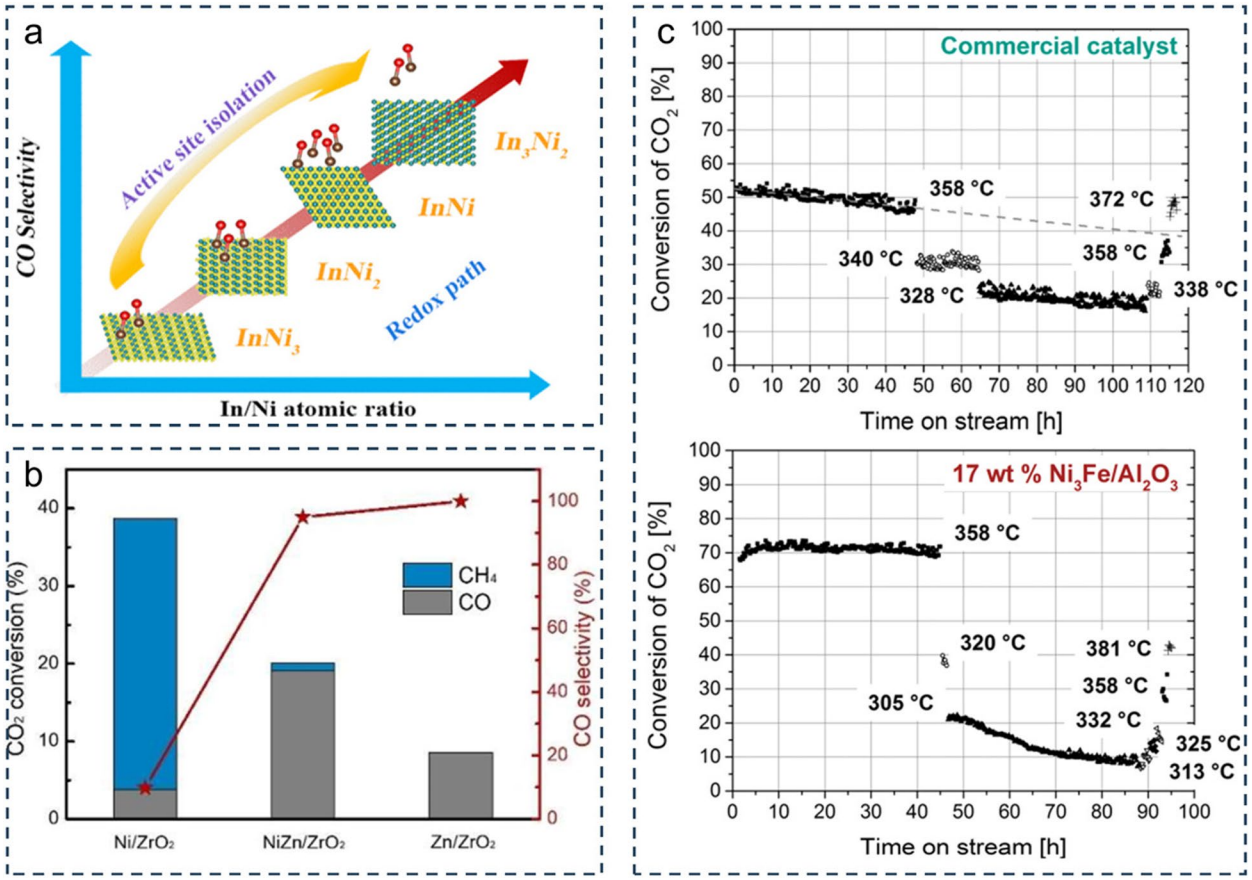

Fig. 4 **a** CO selectivity varying with the In/Ni atomic ratio. **b** CO_2 conversion and CO selectivity for CO_2 hydrogenation over different catalysts at 400 °C. **c** CO_2 conversion of the commercial Ni-based methanation and 17 wt % Ni_3Fe/Al_2O_3 catalysts. Reprinted with permission from Refs. [58, 59], and [60], Copyright 2022, 2022, and 2017, American Chemical Society, Wiley–VCH Verlag GmbH & Co. KGaA, Weinheim, and American Chemical Society

oxygen vacancies. These results unravel the active site dependent catalytic mechanism tuned by surface oxygen vacancies for CO_2 hydrogenation.

According to Wulff's rule [97], the morphology determines the exposed facets that affect their surface compositions and structures. It is therefore that the morphology effect, also called crystal plane effect, of oxide supports has been extensively investigated in heterogeneous catalysis [98–116], including CO_2 hydrogenation [23, 24, 73–80]. As one of the commonly-used oxides, the morphology-dependent catalysis of CeO_2-based catalysts in CO_2 hydrogenation has been frequently observed over a variety of supported metals including Ru, Ni, Co and Rh [24, 73–78, 80]. Wang et al. [73] found the oxygen vacancies in CeO_2-based catalysts playing a crucial role in CO_2 hydrogenation, serving as the active site for CO_2 activation and thus significantly enhancing the low-temperature catalytic activity. By preparing different CeO_2 nanocrystal supported Ru catalysts including nanocubes (r-CeO_2), nanorods (r-CeO_2), and nanopolyhedra (p-CeO_2) dominantly exposing {100}, {110}, and {111} facets, they demonstrated that the supported Ru NPs could promote the formation of oxygen vacancies in c-CeO_2, resulting in the highest reaction rate observed over Ru/c-CeO_2 catalyst. Differently, the best catalytic performance was observed over r-CeO_2 for CeO_2-supported Co, Ni or Rh catalysts [24, 73–80]. In Xie et al.'s study [76], the superior performance over Co/r-CeO_2 catalyst could be correlated to the oxygen vacancies and strong Co-CeO_2 interactions that promote the formation of Co^0 active species, while the solid frustrated Lewis pair (FLP) structures are preferentially formed over Ni/r-CeO_2 catalyst that act as the active sites for enhanced catalytic performance in CO_2 hydrogenation.

In our previous report [24], an incipient wetness impregnation method was employed to synthesis the Rh/CeO_2 catalysts with different CeO_2 morphologies and Rh loadings of around 2 wt. %. Microscopic characterization results reveal the original CeO_2 morphologies unchanged after Rh loadings with an averaged

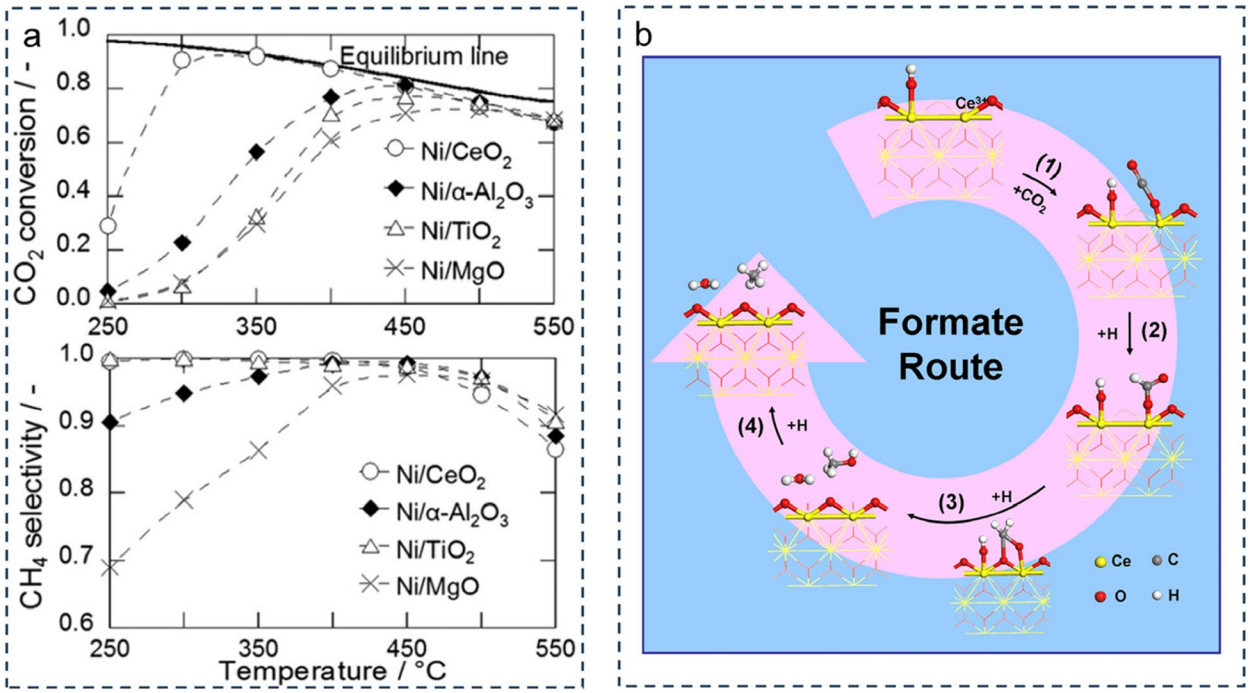

Fig. 5 **a** Effect of support materials on CO_2 conversion and CH_4 selectivity over Ni/CeO_2, Ni/α-Al_2O_3, Ni/TiO_2, and Ni/MgO. **b** Schematic illustration of the formate route for CO_2 methanation over the Ru/CeO_2 catalyst. Reprinted with permission from Refs. [67] and [72], Copyright 2012 and 2016, Elsevier and American Chemical Society

Rh particle sizes of ca. 1.5, 2.1 ± 0.4, and 2.6 ± 0.6 nm over Rh/r-CeO_2, Rh/c-CeO_2, and Rh/p-CeO_2 catalysts, respectively (Fig. 6a1-a3). The catalytic performance of these Rh/CeO_2 catalysts in CO_2 hydrogenation present an order of Rh/r-CeO_2 > Rh/c-CeO_2 > Rh/p-CeO_2 (Fig. 6b), and CH_4 is the exclusive product with the selectivities of nearly 100% (Fig. 6c). However, the intrinsically catalytic performance is very similar over three Rh/CeO_2 catalysts (Fig. 6d), indicating that the different catalytic activity over these Rh/CeO_2 catalysts could be associated with the different density instead of the intrinsic structure of the active sites. Kinetic experiments (Fig. 6e and f) indicate the catalytic performance is determined by the adsorption and activation of CO_2, which is further verified by spectroscopic characterizations to exhibit identical interfacial oxygen vacancy concentrations to their catalytic activity (Fig. 6g). These clearly demonstrate the Rh/CeO_2-catalyzed CO_2 hydrogenation is determined by interfacial oxygen vacancies that varies with the CeO_2 morphologies.

It is widely accepted that the composite oxides generally possess advantages by inheriting favorable properties of the individual metal oxide supports [72, 81–88]. Taking Al_2O_3 support as an example [87], the introduction of CeO_2 into the Ni/Al_2O_3 catalysts can remarkably improve the reducibility by altering the Ni-Al_2O_3 interactions. However, the introduction of TiO_x species or ZrO_2 was found to greatly suppress the formation of $NiAl_2O_3$ spinel phase and weaken the Ni-Al_2O_3 interactions, resulting in more Ni species exposed and thus promoting the CO_2 adsorption capacity. Additionally, it was also found that the Ti^{4+}/Ti^{3+} pairs can contribute to an electron transfer that increases the electron cloud density of supported Ni species and thus facilitates the CO_2 dissociation on catalyst surface. Therefore, the formation of the composite oxides can efficiently improve the catalytic performance of oxide-supported metal catalysts via the modifications of the reducibility, chemisorption capacity, or dispersion of the active species.

2.3 Strong metal-support interactions

The MSIs widespreadly exist for all the supported metal catalysts in different forms, nonetheless, the strength was strongly influenced by various factors, including the electronic properties and geometric structures of oxide support and supported metal NPs as well as their exiting conditions [33, 107]. It has been widely reported that the metal-oxide interfacial structures strongly depend on the MSIs involving diversity electronic transfers and structural evolutions [89, 90, 117]. Consequently, the interfacial catalysis dynamically varies with the MSIs. In other words, optimizing the MSIs could become a

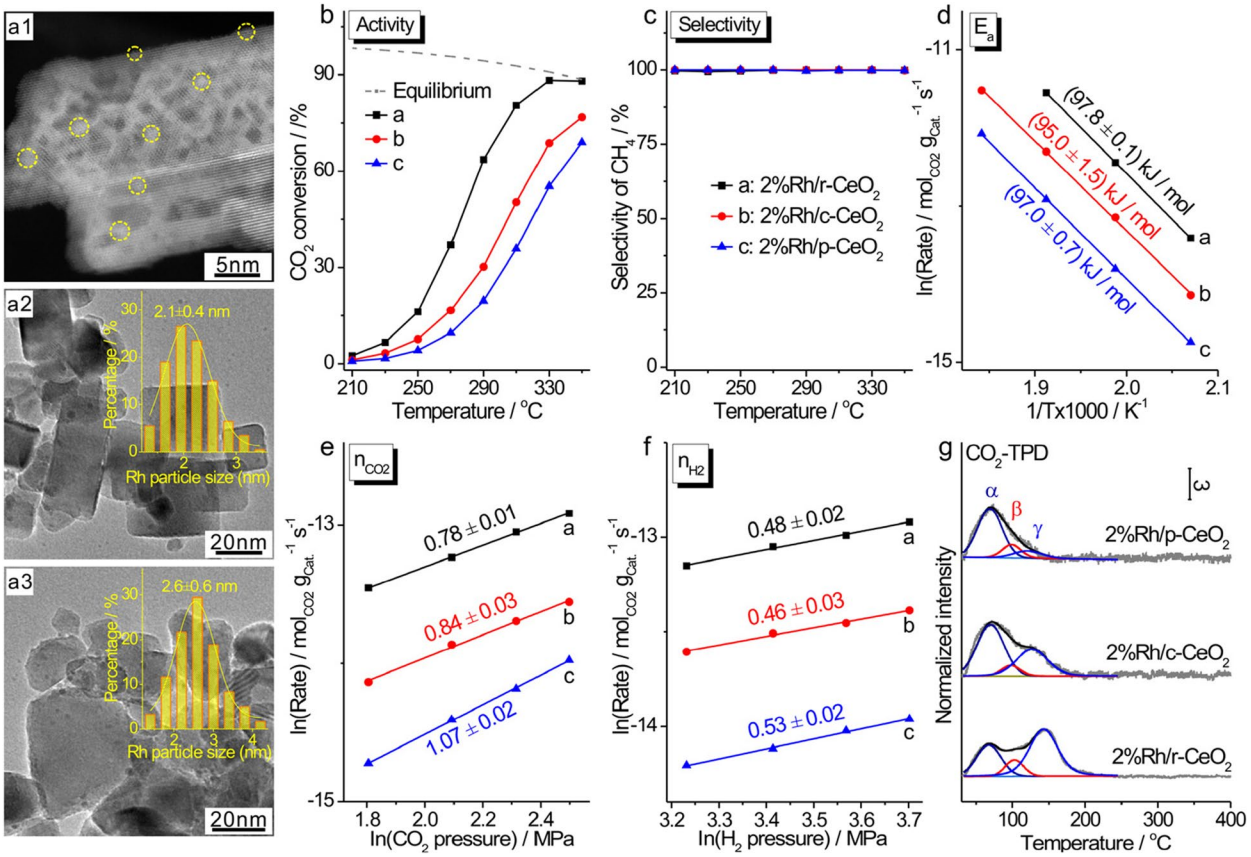

Fig. 6 (a1-a3) Representative TEM images with corresponding size distributions of Rh nanoparticles. (b) Catalytic activity, (c) CH_4 selectivity, (d) Arrhenius plots, reaction orders of (e) CO_2 and (f) H_2 at 230 °C, and (g) CO_2-TPD profiles of various 2%Rh/CeO_2 catalysts. Reprinted with permission from Ref. [24], Copyright 2023, American Chemical Society

superb strategy to tune the metal-oxide interfacial structures and thus their catalytic performance of oxide-supported metal catalysts. Parastaev et al. [89] developed an approach to tune the MSIs via varying the particle size of the support. They prepared a series of ceria-zirconia supported Co catalysts (CoCZ) and the particle size of ceria-zirconia support was varied in a range of 9–120 nm by changing the calcined temperatures of the initial precipitation (Fig. 7a-c). A volcano-like activity trend in CO_2 hydrogenation appears with the calcination temperature, at which the CoCZ700 catalyst with an intermediate CZ particle size of ~ 20 nm exhibits the best activity (Fig. 7c and d). The CO_2 conversion at 225 °C for CoCZ700 catalyst is ca. 2.9 and 5.8 times higher than those for CoCZ1000 and CoCZ500 catalysts. The characterization results reveal that an optimal strength of the Co-CZ interactions could result in the enhanced stability of supported Co NPs during the reduction conditions. With such an optimal MSI, reverse oxygen spillover from the support during reduction treatment is beneficial for the facile formation of oxygen vacancies in ceria that contributes to the dissociation of CO_2 and thus becomes pivotal for the high activity of CO_2 hydrogenation to CH_4 (Fig. 7e).

Moreover, strong metal-support interactions (SMSIs) referred to the migration of support-involved species over the supported metal NPs to produce ultrathin encapsulation overlayers, have also been widely observed in atmospheric CO_2 hydrogenation, which contribute to the enhancements of activity, selectivity towards the target product, and stability [91–96]. Typically, this process emerges in reducible oxide-supported group VIII metals during thermal pretreatments at high temperatures in a specific atmosphere such as H_2, CO, or O_2 [91–96, 118, 119]. For example, a co-reduction strategy in H_2 atmosphere was used to prepare the encapsulation of the TiO_x overlayers on metallic Ru NPs via the improved SMSIs over Ru/TiO_2 catalysts with the formation of $Ru_xTi_{2-x}O_2$ oxide interphase by increasing the calcination temperature (Fig. 8a) [92], which exhibits a superior activity in CO_2 hydrogenation with a CH_4 selectivity of 100%. Additionally, the SMSIs often happen upon the reaction

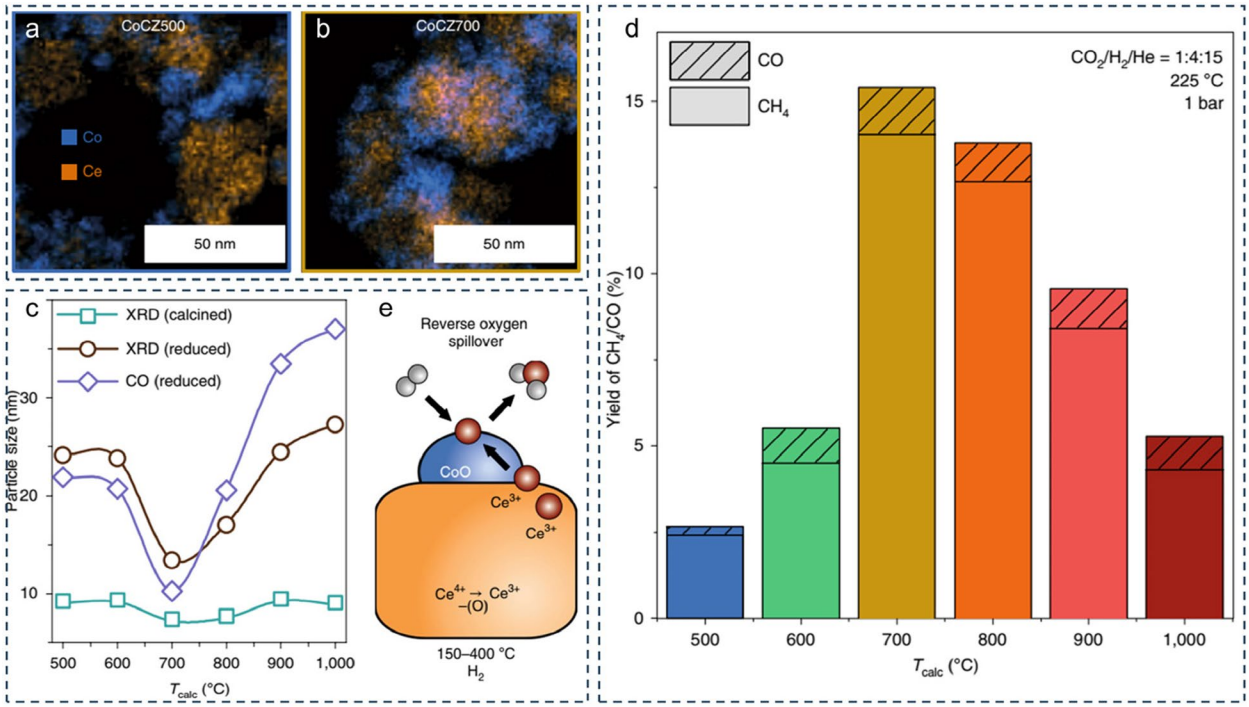

Fig. 7 EDX mapping of as-prepared **a** CoCZ500 and **b** CoCZ700. **c** Cobalt particle size estimated by X-ray diffraction for calcined and reduced samples and by CO chemisorption for reduced samples. **d** Catalytic performance at 225 °C of cobalt-based catalysts supported on CZ calcined at different calcination temperatures. **e** Schematic representation of the reverse oxygen spillover effects in the CoCZ700 catalyst. Reprinted with permission from Ref. [89], Copyright 2020, Nature Publishing Group

conditions induced by the reactant or product molecules on catalyst surfaces at high temperature, which could give rise to different catalytic modes in CO_2 hydrogenation. Xin et al. [93] reported an adsorbate-induced SMSI structure over Ru-MoO_3 catalyst by a CO_2-H_2 mixture gas that enables dynamic tuning of the catalytic selectivity in CO_2 hydrogenation. During the reaction, the MoO_3 support is reduced below 500 °C via the promotion effect of Ru NPs to generate active MoO_{3-x} overlays with rich oxygen vacancies covered over Ru NPs, i.e. the Ru@MoO_{3-x} structure (Fig. 8b), which leads to the occurrence of different catalytic reaction in CO_2 hydrogenation compared to unencapsulated Ru-MoO_3 structure. A CH_4 selectivity of 100% generated by the Sabatier reaction is acquired on the unencapsulated Ru-MoO_3 structure while the Ru@MoO_{3-x} structure facilitates the RWGS reaction to generate CO with a selectivity of above 99% (Fig. 8c). Spectroscopic characterizations together with DFT calculations demonstrate such sensitive changes of catalytic selectivity arising from the different exposed surface sites, in which the Sabatier reaction mostly occurs over the exposed Rh sites over unencapsulated Ru-MoO_3 structure, however, the MoO_{3-x} overlayers over Ru@MoO_{3-x} structure with rich oxygen vacancies facilitate the RWGS reaction. Compared between the MSIs and SMSI effects, the MSIs are more easily to occur over metal/oxide catalysts. For instance, ZrO_2, as a weak reducible support, can promote the MSIs but suppress the SMSI effect, contributing to the charge transfer from oxygen vacancies in the ZrO_x surface region to adjacent Ru NPs, which finally lead to strong Ru-CO bonding and enhanced CH_4 production [120]. These results nicely confirm the metal-oxide interfacial structures strongly dependent on the (S)MSIs.

3 Formic acid / Formate

As one of the important commodity chemicals, FA and its derivative (formate) exhibit a diversity of applications in chemical industry such as medical, leather, and preservation [121, 122]. Traditionally, the FA production arises from either the oxidation of biomass or the hydrolysis of methyl formate [123, 124], which is uneconomical due to the introduction of some unexpected by-products that are separated difficultly. An efficient strategy to address this issue is to develop new and sustainable catalytic routes to produce FA/formate. Catalytic CO_2 hydrogenation to FA/formate is regarded as an excellent approach, which not only utilizes the greenhouse gas of CO_2 caused by the massive utilization of fossil fuels, but also produce FA/formate without the generation of other

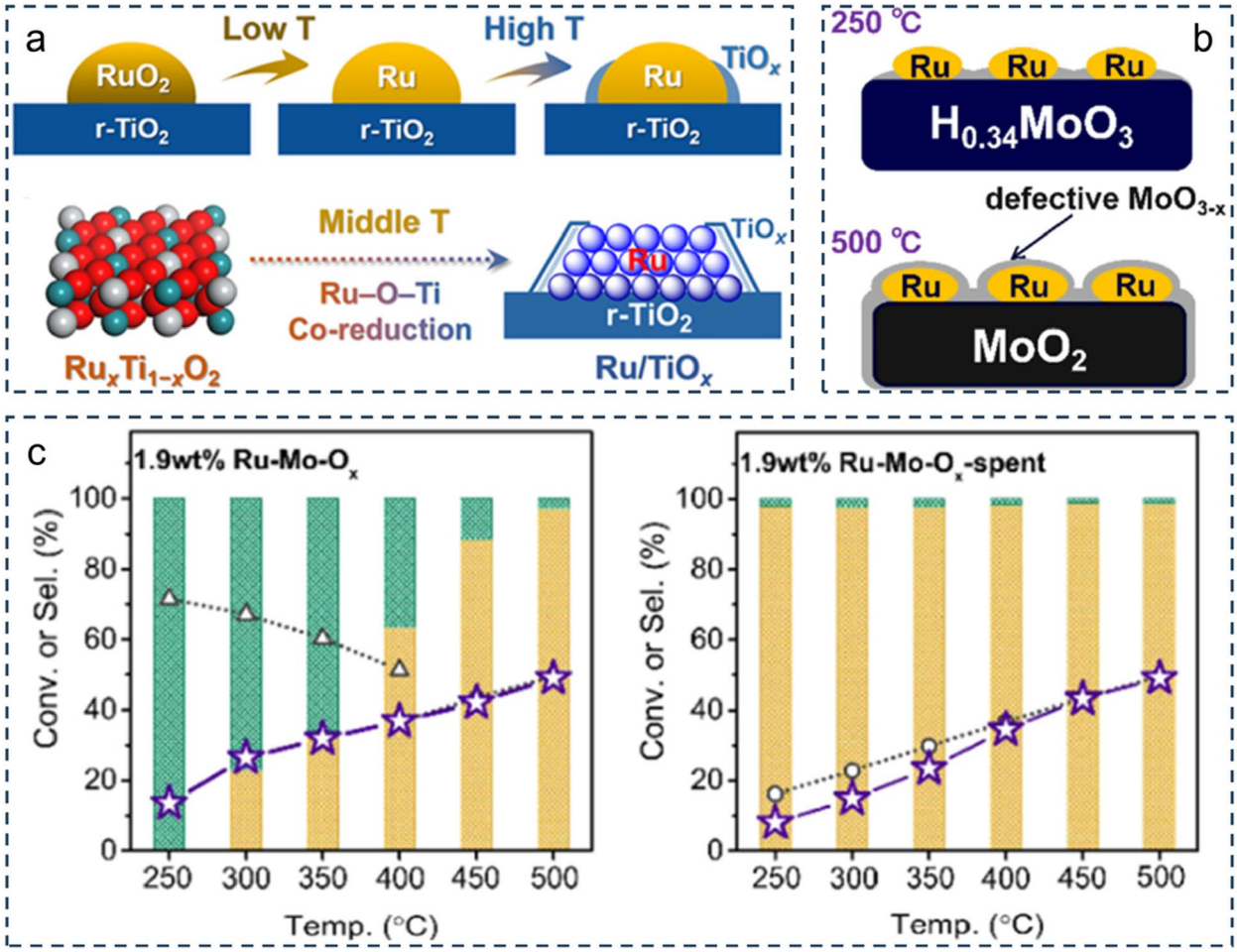

Fig. 8 **a** Classic support migration mechanism for SMSI formation, as in the case of the Ru/TiO_2-200Air sample and proposed Ru–O-Ti co-reduction mechanism for the facile formation of SMSI, as in the case of the Ru/TiO_2-xAir (x = 300, 400, or 500 °C) samples. **b** Schematic diagrams of the 1.9 wt % Ru-Mo-O_x-250 and 1.9 wt % Ru-Mo-O_x-500 catalysts. **c** Catalytic performance evolution of the Ru-Mo-oxide catalysts in CO2 hydrogenation: fresh 1.9 wt %Ru-Mo-O_x catalyst and spent catalyst after the reaction in 1.9 wt %Ru-Mo-O_x-spent. Reprinted with permission from Refs. [92] and [93], Copyright 2022, American Chemical Society

by-products because such a reaction is atomically economical ($CO_2 + H_2 \rightarrow HCOOH$). Meanwhile, the FA/formate product is also an important material for hydrogen storage that is beneficial for the realization of CO_2-mediated hydrogen energy cycle [125, 126]. Thermodynamically, the direct CO_2 hydrogenation to FA/formate is unfavorable (Eq. 3, $\Delta G = 33$ kJ mol^{-1}), but can be proceeded in aqueous solution (Eq. 4, $\Delta G = -4$ kJ mol^{-1}). Moreover, this reaction could be further promoted with the addition of bases such as bi/carbonates, hydroxides, and amines due to the efficient suppression of the reverse reactions containing the dehydration/dehydrogenation of FA [127–129]. Therefore, the development of efficient catalysts for FA/formate production from CO_2 hydrogenation is of great significance and high desire.

$$CO_2(g) + H_2(g) \rightarrow HCOOH(1)(\Delta H_{298K} = 33 \text{ kJ mol}^{-1}) \quad (3)$$

$$CO_2(aq) + H_2(aq) \rightarrow HCOOH(1)(\Delta H_{298K} = -4 \text{ kJ mol}^{-1}) \quad (4)$$

Previously, significant efforts have been devoted to develop efficient homogeneous catalysts for FA/formate production from CO_2 hydrogenation which are mainly focused on homogeneous transition metal complexes based on Rh, Ru, Ir, and Fe [130–132]. Although high FA/formate productivity is acquired using homogeneous catalysts, unfortunately, high costs and tedious separations for catalyst reproduction seriously limit this process. By contrast, heterogeneous catalysts that can remedy these drawbacks that have aroused considerable interests. Among various heterogeneous catalysts reported in literature [133–141], supported-Pd catalysts

exhibit exceptional activity and become the most promising, generally more than one order of magnitude performance than other supported metal catalysts [133–136]. However, their catalytic performance is still inferior in comparison to homogeneous catalysts, which limits the applications. It has been widely reported that the catalysis of supported Pd catalysts in CO_2 hydrogenation to FA/formate arises from the synergetic effect between Pd and support, in which Pd is responsible for the H_2 dissociation while the adsorption and activation of CO_2 generally occur on the support [136, 142–145]. Therefore, tuning the structures of Pd and support are crucial in affecting the kinetic equilibrium and thus the catalytic activity.

3.1 The electronic structure of supported Pd species

As one of two pivotal reaction sites, supported Pd species is responsible for the adsorption and activation of H_2 and thus strongly affects the hydrogenation performance [142]. Theoretically, reducing the metal particle size to expose more surface sites can promote the catalytic reaction. However, such a strategy is not suitable for supported Pd catalysts in CO_2 hydrogenation to FA/formate. Previous studies indicated the electronic properties of supported Pd species acting as the key role in this reaction [136, 142–146], which has an intrinsic influence on catalytic hydrogenation performance. For instance, in Pd/CeO_2 catalyzed CO_2 hydrogenation to FA [142], the electronic structures of supported Pd species were finely tailored by altering the Pd loading to generate changing Pd particle sizes from atomic dispersion to large NPs (ca. 3.4 nm). The TOF value calculated on basis of surface Pd atoms over large Pd NPs is more than 9 times higher than that over atomically dispersed Pd atoms, indicating that metallic Pd species is more beneficial for the adsorption and activation of H_2 and thus the hydrogenation performance. Similar results were also observed on Pd/ZnO, Pd/ZrO_2, and Pd/TiO_2 catalysts [136, 143, 144].

In addition to the electronic properties modified by altering the particle size, the bimetal alloy can be also employed to tune the electronic properties of supported Pd species [147, 148]. It is thus regarded as an efficient approach to boost the catalytic activity by introducing a weakly-electronegative metal atoms to increase Pd metallicity such as Ag, Cu, Mn, and Co [134, 135, 149–155]. Sun et al. prepared the zeolite-encaged Pd-Mn nanocatalysts for CO_2 hydrogenation to formate [134]. The results demonstrated the introduction of Mn atoms greatly improving the metallicity of supported Pd atoms which results in an unprecedented high formate generation rate of 2151 $mol_{formate}$ mol_{Pd}^{-1} h^{-1} at 353 K over $PdMn_{0.6}$@S-1 catalyst (Fig. 9a). However, the precise structures are still ambiguous due to the alloy complexity. To catch this point, Mori et al. [135] prepared a series of TiO_2-supported PdAg catalysts with different PdAg alloy structures including Pd covered on Ag (Ag@Pd), Ag covered on Pd (Pd@Ag), and PdAg mixed uniformly. Compared to monometallic Pd/TiO_2 catalyst, the improved catalytic activities were observed for all $Pd–Ag/TiO_2$ catalysts, among which the $Pd@Ag/TiO_2$ catalyst exhibits a maximum turnover number of 14,839 calculated on basis of surface Pd atoms that is more than tenfold increase in comparison to corresponding Pd/TiO_2 catalyst (Fig. 9b). The CO-DRIFTS spectra coupling with Pd 3d XPS spectra (Fig. 9c and d) demonstrate the decreased electron density of active Pd atoms observed for all TiO_2-supported PdAg catalysts, which results from a synergistic effect of Pd atoms alloying with Ag atoms. Meanwhile, the strongest metallicity emerges over $Pd@Ag/TiO_2$ catalyst (Fig. 9e), which contributes to the facilitation of the hydrogenation step of adsorbed HCO_3^- species that is rate-determining for formate production (Fig. 9f), resulting in the highest formate production observed. These results elucidate the importance of tailoring the electronic properties of supported Pd species in CO_2 hydrogenation to FA/formate.

3.2 The nature of the oxide supports

As mentioned above, the support plays a crucial role in CO_2 hydrogenation to FA/formate, which can not only govern the adsorption and activation of CO_2 that is responsible for the reaction activity, but also tailors the electronic properties of supported Pd species via the MSIs that is influential to H_2 dissociation and hydrogenation process, jointly contributing to the catalytic performance [136, 142–145]. During a long period, the carbon-based supports such as active carbon and carbon nitride are considered as the best category supports for FA/formate production, which generally exhibit high activities and recycle stabilities compared to other supported catalysts [133, 156–158]. Recently, another class of supports called metal oxides also exhibit great potential in this reaction in view of their versatile redox/acid–base properties and high stability. In contrast to numerous studies on the carbon-based supports, the metal oxide supports with high catalytic performance are few demonstrated for CO_2 hydrogenation, mainly focused on some reducible oxides like TiO_2, CeO_2 and ZrO_2 with rich surface oxygen vacancies capable of adsorption and activation of CO_2 upon reduction [135, 136, 142–145]. It has been confirmed that the nature of oxide supports including the type [142], crystal phase [143] and morphology/crystal plane [136, 144, 145] has a significant effect on the catalytic performance, which will be detailedly introduced below.

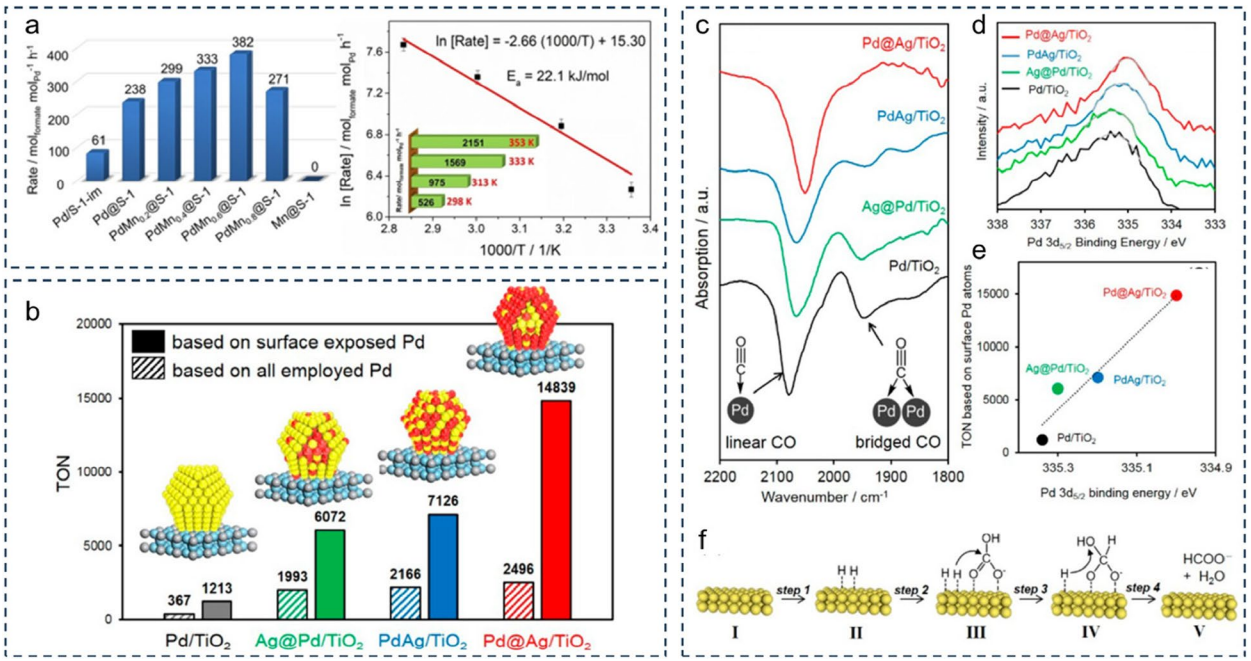

Fig. 9 **a** Comparison of the formate generation rates from the CO_2 hydrogenation over various catalysts and CO_2 hydrogenation over the $PdMn_{0.6}$@S-1 catalyst in the NaOH solution at different temperatures. **b** Comparison of the catalytic activities of a series of supported PdAg catalysts with different surface compositions and Pd/TiO_2 during CO_2 hydrogenation. **c** FT-IR spectra of CO chemisorbed on Pd and PdAg samples. **d** XPS spectra of Pd and PdAg samples. **e** Relationship between the TON for CO_2 hydrogenation based on surface-exposed Pd atoms (as determined by CO pulse adsorption) and the Pd 3d binding energy (as determined by XPS). **f** Possible reaction mechanism. Reprinted with permission from Refs. [134] and [135], Copyright 2020 and 2018, Wiley–VCH Verlag GmbH & Co. KGaA, Weinheim and American Chemical Society

Previously, it was commonly believed that the catalytic activity for oxide-supported Pd catalysts is inferior to Pd deposited on carbon-based supports until the results reported by ours using Pd/TiO_2 catalysts with both the surface basicity and the H_2 activation capacity tailored finely [142]. We first prepared a series of Pd/CeO_2 and Pd/ZnO catalysts with changing Pd particle size, taking as model catalysts. An adverse variation trend with the Pd particle size was observed on two different oxide supports (Fig. 10a). Interestingly, the calculated TOF values are similar over Pd/ZnO catalysts but different distinctly over Pd/CeO_2 catalysts (Fig. 10b). These suggest the type of oxide supports strongly affecting the catalytic behaviors. The kinetic results together with in situ DRIFTS spectra demonstrate the bidentate carbonate and bicarbonate species serving as the key intermediates for formate production (Fig. 10c). For Pd/ZnO catalysts with barren basic properties, the adsorption and activation of CO_2 are seriously limited to suppress the generations of surface carbonaceous species, consequently, the CO_2 activation to yield surface carbonaceous species is the RDS and thus the catalytic performance is less affected by the electronic properties of supported Pd species (Fig. 10d). In contrast, the RDS is switched to the hydrogenation of surface carbonaceous species over Pd/CeO_2 catalysts due to the abundant surface basic sites of CeO_2 that can accelerate the CO_2 conversion to carbonaceous species. As a result, the catalytic activity is strongly dependent on the electronic structures of supported Pd species that are responsible for the H_2 dissociation and hydrogenation process (Fig. 10d). Based on these results, we found that the FA/formate formation from CO_2 hydrogenation is determined by two crucial parameters, i.e. the surface basic sites and the electronic properties of supported Pd species, which are responsible for CO_2 activation and H_2 dissociation, respectively. By these principles, a highly efficient Pd catalyst with an averaged particle size of 4.6 nm deposited on TiO_2 featuring strongly basicity than CeO_2 was developed to afford a TOF of up to 909 h^{-1} at 40 °C (Fig. 10e), far higher than that on Pd/CeO_2 catalysts and even comparable to the top results reported on carbon-based supports [133, 156–158]. These clearly reveal the importance of choosing a suitable oxide support for FA/formate production from CO_2 hydrogenation.

Following up this thought, we further prepared a series of Pd/ZrO_2 catalysts for CO_2 hydrogenation to formate [143], whose structures are tuned by altering

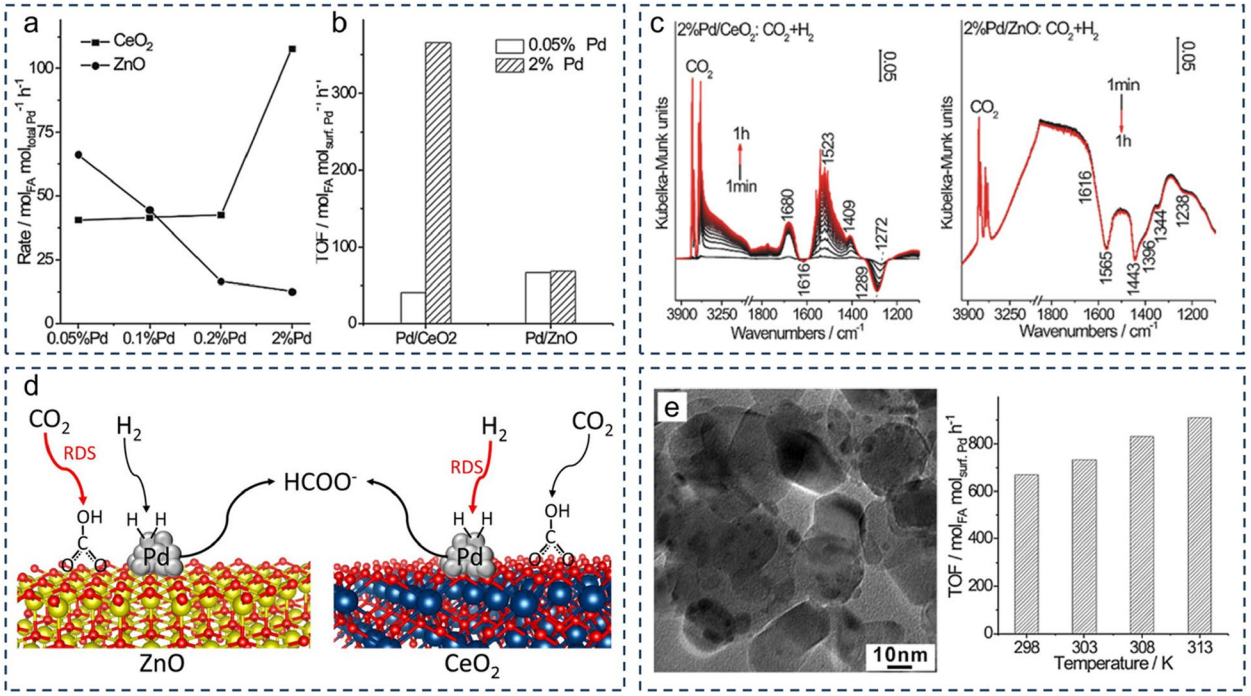

Fig. 10 **a** Formation rate of FA calculated by total Pd atoms on various Pd loadings of Pd/CeO_2 and Pd/ZnO catalysts at 373 K; **b** TOFs of FA calculated by surface Pd atoms on 0.05%Pd/CeO_2, 2%Pd/CeO_2, 0.05%Pd/ZnO, and 2%Pd/ZnO catalysts at 373 K. **c** In situ DRIFTS spectra of CO_2 hydrogenation reaction under an atmosphere of CO_2 and H_2 (1:1) on 2%Pd/CeO_2 and 2%Pd/ZnO catalysts at 373 K. **d** Proposed reaction mechanism of CO_2 hydrogenation to formate over Pd/CeO_2 and Pd/ZnO catalysts. **e** Representative TEM images and TOFs for the FA production calculated by surface Pd atoms on 2%Pd/TiO_2 catalyst. Reprinted with permission from Ref. [142], Copyright 2019, Elsevier

the crystal phase of ZrO_2 supports including monoclinic ZrO_2 (ZrO_2-M), tetragonal ZrO_2 (ZrO_2-T), and hybrid ZrO_2 (ZrO_2-M&T) (Fig. 11a). Due to the distinctly different surface basicity, a remarkable dependence of the catalytic activity on the crystal plane of ZrO_2 was observed for three Pd/ZrO_2 catalysts, among which Pd/ZrO_2-T catalyst displays the best activity with a TOF value of up to ca. 2817 h^{-1} at 100 °C (Fig. 11b and c). Kinetic studies coupling with in situ DRIFTS spectra unveil the activation of CO_2 as the key step in determining the reaction activity and thus regarded as the RDS. As a result, the highest concentration of surface basicity over ZrO_2-T and Pd/ZrO_2-T catalysts enable enough surface sites to activate CO_2 that is responsible for the excellent activity of Pd/ZrO_2-T catalyst in CO_2 hydrogenation to formate (Fig. 11d).

Analogously, the morphology/crystal plane of oxide supports also strikingly affect the catalytic activity of supported Pd catalysts for FA/formate production, as verified over CeO_2, ZnO, and TiO_2 supports [136, 144, 145]. A typical example is the Pd/TiO_2 catalyzed CO_2 hydrogenation to formate [136], where a morphology-engineered strategy was employed to develop improved Pd/TiO_2 catalyst with extremely high activity and recycle stability. Three types of anatase TiO_2 nanocrystals predominantly exposing {001}, {100}, or {101} facets were used as supports to synthesize Pd/TiO_2 catalysts for CO_2 hydrogenation to formate and morphology-dependent catalysis was observed (Fig. 12a-c). Compared to Pd/TiO_2{101} and Pd/TiO_2{001} catalysts, Pd/TiO_2{100} catalyst exhibits an unprecedentedly high activity, giving a TOF value of up to ca. 1369 h^{-1} at 40 °C (Fig. 12d and e), and keeps stable with seldom unchanged activity after 6 cycles (Fig. 12f). The characterization results (Fig. 12 g-i) demonstrate that the excellent activity over Pd/TiO_2{100} catalyst is ascribed to its high density of moderate basic sites and relatively more surface Pd(0) species, responsible for CO_2 and H_2 activations, respectively, while high oxygen vacancy concentrations in TiO_2{100} support are beneficial for the Pd-TiO_2 interactions that can stabilize Pd structures and thus contributing to the catalytic stability. The above reports highlight the importance of the nature of oxide supports in FA/formate formation and demonstrate the possibilities of tailoring the oxide structures for developing efficient supported Pd catalysts for CO_2 hydrogenation.

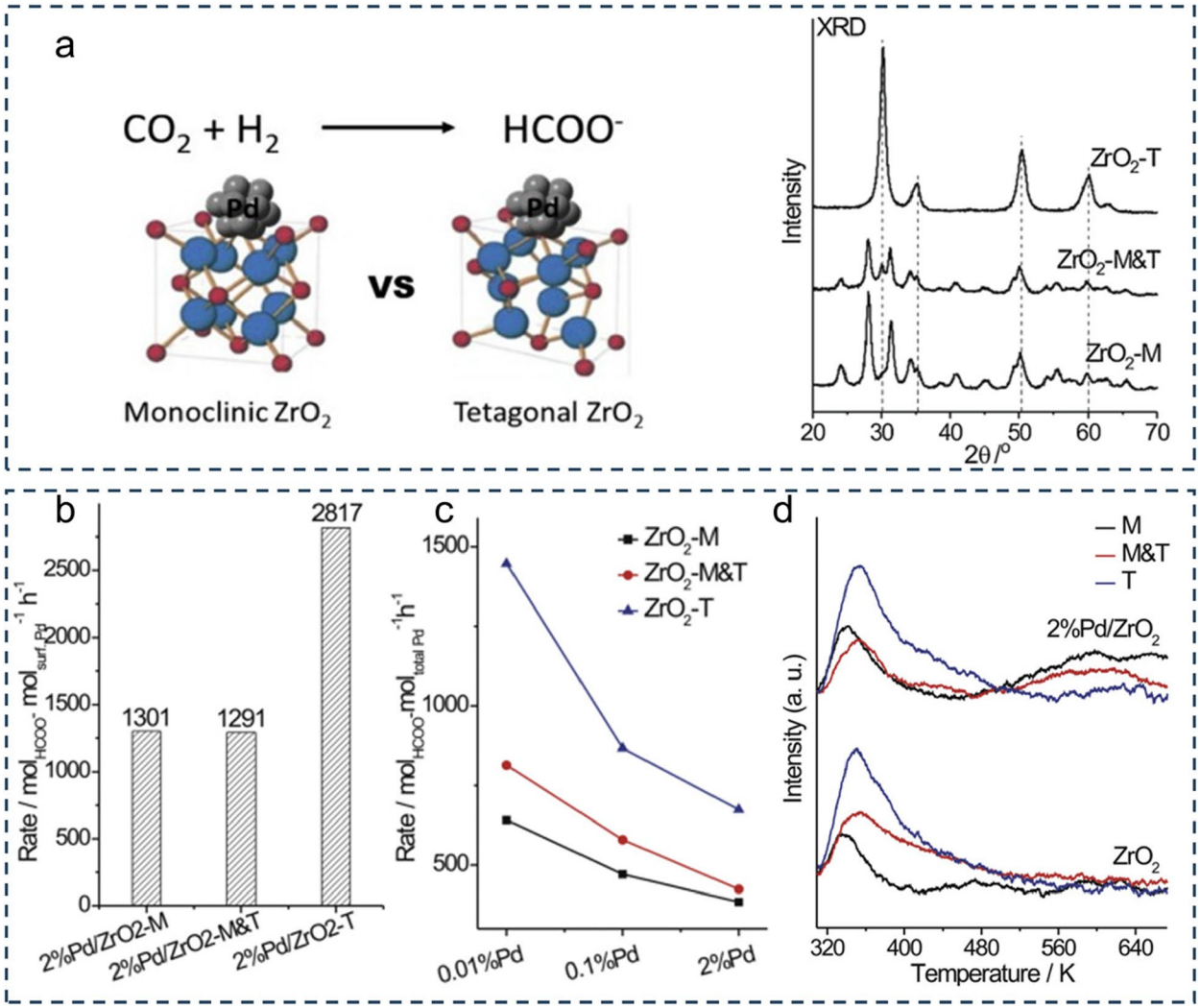

Fig. 11 **a** Models of different ZrO_2-supported Pd for CO_2 hydrogenation to formate and XRD patterns of various ZrO_2 supports. Production rate of formate on various Pd/ZrO_2 catalysts based on the **b** total amount of Pd atoms and **c** surface Pd atoms. **d** CO_2-TPD profiles of various ZrO_2 and Pd/ZrO_2 catalysts. Reprinted with permission from Ref. [143], Copyright 2019, Elsevier

4 Methanol

As one of the top five commodity chemicals around the world, methanol (CH_3OH) has been widely used as a solvent, an alternative fuel, and an important intermediate in chemical industry for the production of a diversity of chemicals such as olefins, acetic acid, and methyl tert-butyl ether [159, 160]. Historically, methanol was first obtained from the charcoal production by wood as a byproduct and thus called wood alcohol [159]. Until the 1920s, a commercial schema was developed by the syngas-to-methanol synthesis process using ZnO-Cr_2O_3 catalysts operating at 320–450 °C and 250–350 bar [15]. Later on, this process was further optimized to conduct under milder reaction conditions of 200–300 °C and 50–100 bar over Cu/ZnO/Al_2O_3 catalysts [161]. Nowadays, as an alternative feedstock, the carbon source of methanol synthesis in syngas atmosphere (CO) could be replaced by CO_2 that has also been considered as an efficient approach for CO_2 utilization [162].

During CO_2 hydrogenation to methanol (Eq. 5), a competing RWGS reaction (Eq. 6) could be occurred [163] that, on the one hand, suppresses the methanol synthesis from direct CO_2 hydrogenation, on the other hand, likely opens a new methanol synthesis way from CO, formed via the RWGS reaction, further hydrogenation (Eq. 7) [164]. In view of thermodynamic point, CO_2 hydrogenation to methanol is exothermal (Eq. 5, ΔH_{298K} = -49.5 kJ mol^{-1}) and decompressive. Thus, the decreased reaction temperature and increased reaction pressure could be favorable for the methanol production.

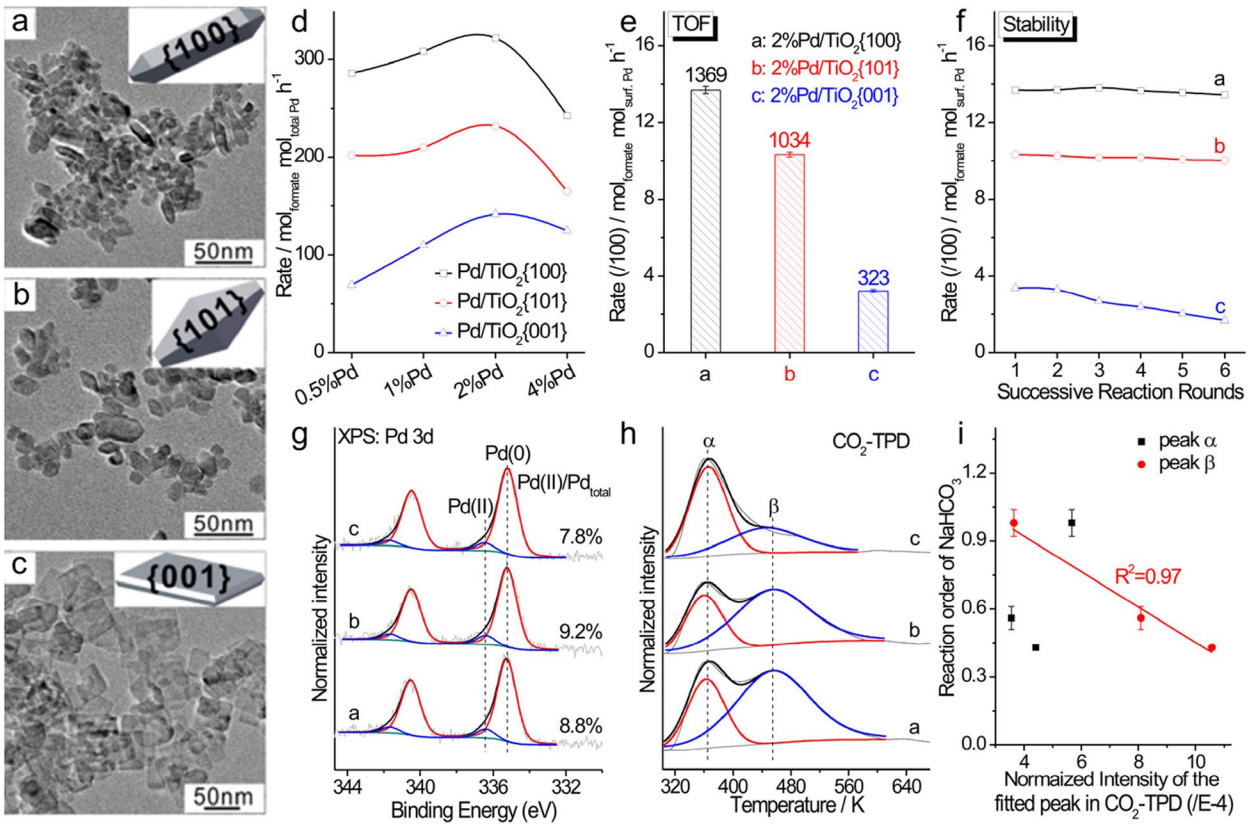

Fig. 12 Representative TEM images with corresponding models f (a) TiO_2{100}, (b) TiO_2{101}, and (c) TiO_2{001} nanocrystals. (d) Production rate of formate calculated by the total amount of Pd atoms on various Pd/TiO_2 catalysts at 313 K; (e) Production rate of formate calculated by the surface amount of Pd atoms on various representative $2\%Pd/TiO_2$ catalysts at 313 K and corresponding (f) course of successive reaction rounds. (g) Pd 3d XPS spectra without exposure to air and (h) CO_2-TPD profiles of various 2%Pd/TiO2 catalysts. (i) Reaction order of $NaHCO_3$ of various $2\%Pd/TiO_2$ catalysts over CO_2 hydrogenation into formate as a function of the intensity of the fitted peak α and β normalized by the specific BET surface area in CO_2-TPD results, respectively. Reprinted with permission from Ref. [136], Copyright 2022, Elsevier

However, enhanced reaction temperature promotes the CO_2 activation that takes advantage of the kinetic modes to accelerate the reaction activity. Unfortunately, the undesired byproducts such as CO and hydrocarbons are also generated. Therefore, tailoring the catalyst structure with both good activity and high selectivity is pivotal form methanol synthesis reaction.

$$CO_2 + 3H_2 \rightarrow CH_3OH + H_2O(\Delta H_{298K} = -49.5\ \text{kJ mol}^{-1}) \quad (5)$$

$$CO_2 + H_2 \rightarrow CO + H_2O(\Delta H_{298K} = 41.2\ \text{kJ mol}^{-1}) \quad (6)$$

$$CO_2 + 2H_2 \rightarrow CH_3OH(\Delta H_{298K} = -90.6\ \text{kJ mol}^{-1} \quad (7)$$

In the past, numerous studies have been devoted to the development of efficient heterogeneous catalysts for CO_2 hydrogenation to methanol and various materials aspects have also been investigated [1, 2, 6, 162, 165–167]. It is well-known that there are two main categories of catalysts in this reaction, i.e. oxide-based catalysts and zeolite-based catalysts, among which the former is considerably desirable in particular the $Cu–ZnO-Al_2O_3$ catalyst that has been commercialized [13–16]. For oxide-based catalysts, the key component is metal-oxide composites, whose interfacial structures strongly affect the catalytic performance [168–172]. The followings provide comprehensive introductions of different structural factors including the type [173–178], the particle size [179–184], the morphology/crystal plane [185–189], and the bimetal synergy [190–195] of the metals, the particle size [196], the crystal phase [197–203], the morphology/crystal plane [174, 204–208], and the composite [30, 209–211] of the oxides, adverse oxide/metal catalysts [172, 187, 212–216], and their (S)MSIs [217–222] on affect the interfacial structures and thus the interfacial catalysis for CO_2 hydrogenation to methanol so as to govern the key elements in determining the activity and selectivity.

4.1 The nature of the metals

Until now, catalytic CO_2 hydrogenation to methanol has been reported on different metal-based catalysts including Cu, Ag, Au, Cd, and Pd [173–178], among which Cu-based catalysts are regarded as the most promising in terms of their excellent catalytic performance and low costs [175, 178]. Thus, the Cu–ZnO-Al_2O_3 catalysts have been commercially employed in this reaction [15, 161]. Typically, a commercial Cu–ZnO-Al_2O_3 catalyst contains ca. 50–70% of CuO (precursor), 20–50% of ZnO and 5–20% of Al_2O_3, where Cu is the main active component, ZnO acts as promoters, and Al_2O_3 enhances the thermal stability. At the initial stage, several studies reported that the methanol synthesis reaction catalyzed by exposed Cu surface is structure-insensitive and thus the catalytic performance presents a linear relationship with Cu surface area [223–227]. However, limited by the measure conditions, the measured Cu surface areas by N_2O titration could result in differences between the measured and the real values of exposed Cu surface areas [228, 229]. Recent studies demonstrated a structure-sensitive reaction observed over Cu-catalyzed methanol synthesis that is strongly dependent the particle sizes and the morphologies/crystal planes of Cu over Cu-based catalysts [181, 183–188].

Altering the Cu particle sizes, both the geometric and the electronic structures are changing correspondingly which will significantly affect the interfacial catalysis of Cu-based catalysts in CO_2 hydrogenation to methanol [181, 183, 184]. This conclusion was comprehensively verified over bare Cu and supported Cu catalysts including Cu/ZnO and Cu/Zn-silicate by Berg et al. [184]. In their study, they prepared a series of Cu and supported Cu catalysts with changing Cu particle sizes range from ca. 2 nm to ca. 15 nm for methanol synthesis reaction. The results display that the formation rates of methanol based on surface Cu atoms (h^{-1}) present similar variation trends to Cu particle sizes over both the Cu and the supported Cu catalysts (Fig. 13). As the increase of Cu particle size, the catalytic performance is prominently enhanced by a factor of ca. 3 with Cu particle size growing up from 2 to 8 nm, and subsequently keeps almost unchanged. This indicates that the methanol synthesis reaction is predominantly taken place at copper surface sites with a unique configuration of Cu atoms such as step-edge sites while finer Cu particles are not accommodated.

The exposed Cu crystal planes are another factor in affecting surface Cu structures in particular Cu coordination numbers [230], resulting in different catalytic behaviors for methanol synthesis [185–189]. For instance, on bare Cu surfaces, the catalytic activity for methanol production was confirmed to follow an order

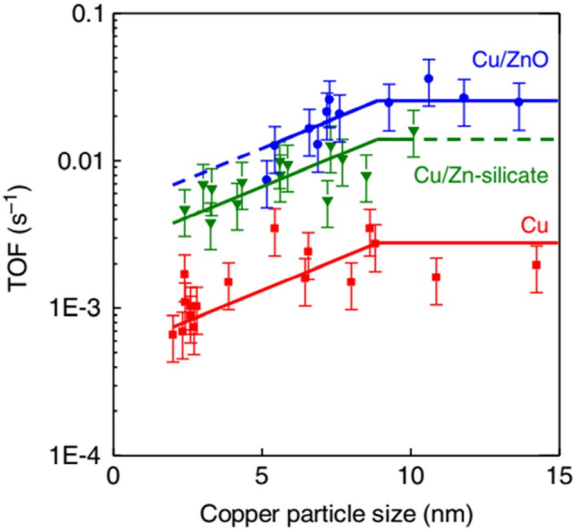

Fig. 13 The surface-specific activity (TOF) for methanol synthesis after 2–10 h on stream at 260 °C and 40 bar plotted as a function of the number-averaged copper particle size for different Cu-containing catalysts. Reprinted with permission from Ref. [184], Copyright 2016, Nature Publishing Group

of Cu(110) > Cu(100) > Cu(111) using single-crystal-based model catalysts [186]. Furthermore, this phenomenon was also extended to ZnO-covered Cu surfaces, with the activity order of ZnO/Cu(100) > ZnO/Cu(111) [187]. Due to the instability of Cu exposed in air, the crystal-plane effect of Cu in methanol synthesis is still unrealized under real reaction conditions until the Cu nanocrystals successfully derived from corresponding Cu_2O nanocrystals during reduction conditions recently [100]. Kordus et al. [189] employed this method to prepare ZnO-supported Cu cube catalysts with partial loss of the Cu(100) facets during CO_2 hydrogenation (Fig. 14a-d). The results solidly demonstrate that ZnO-supported Cu(100) (cubes) catalysts (NC) are more active for methanol production than similarly sized sphere Cu supported on ZnO (NP) and commercial reference catalyst (CR) (Fig. 14e and f). Combined with DFT calculations, the excellent catalytic activity for NC catalyst arises from a weaker adsorption capacity of formate and a lower reaction energy between HCOOH and TS-H_2COOH on ZnCu(100) surface compared to ZnCu(211) surface.

Besides single Cu NPs, the introduction of an additional metal into the catalyst system to form bimetal compounds could greatly boost the catalytic performance [190–195]. Pasupulety et al. [191] studied the influence of Au into the Cu–ZnO-Al_2O_3 catalysts for methanol synthesis and a positive promotion was observed with 1% Au loading, which mainly arises from the formed Cu-Au interfaces that are beneficial for the hydrogen spillover

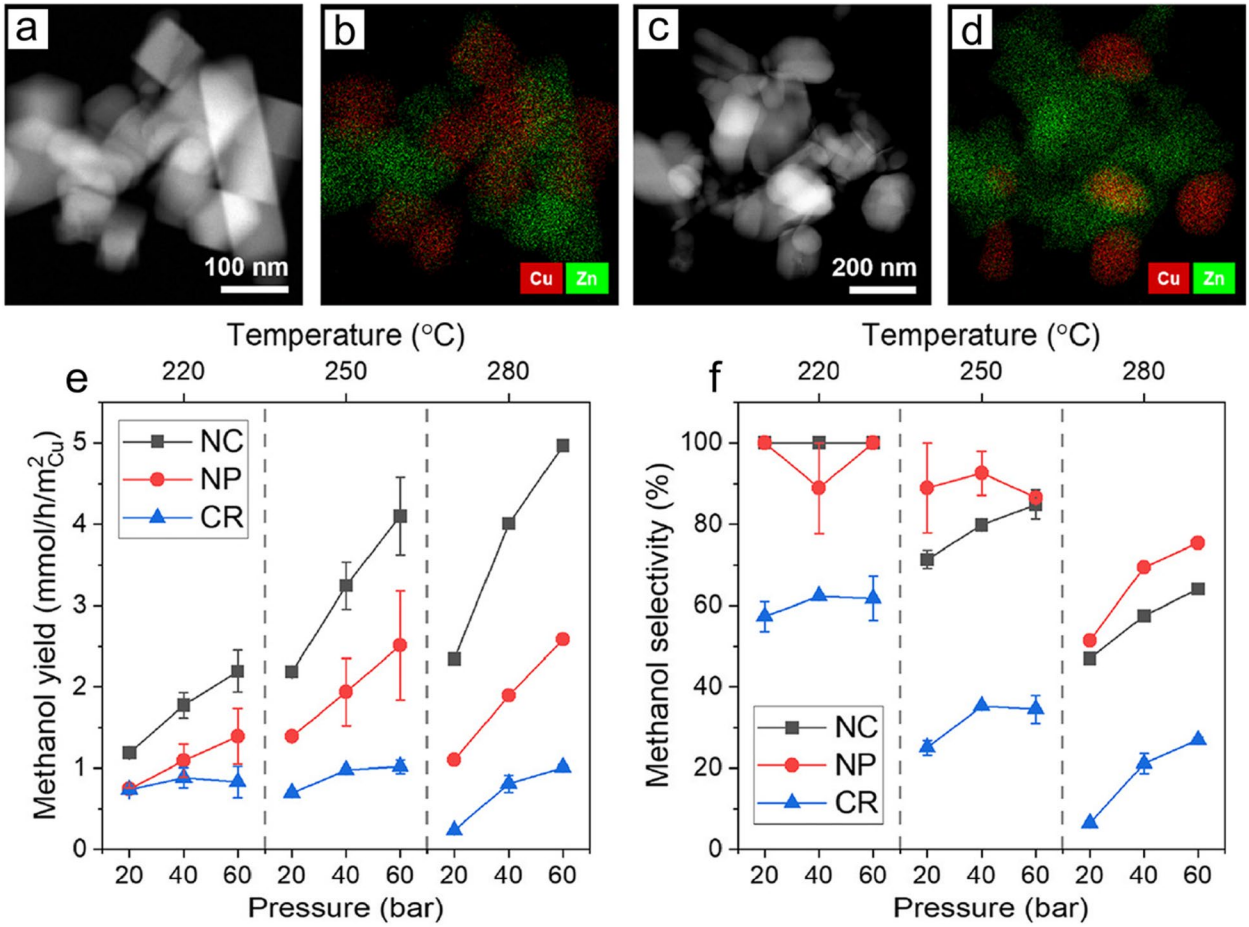

Fig. 14 STEM images and corresponding EDX maps of cubic Cu2O NPs supported on nanocrystalline ZnO: **a**, **b** as prepared Cu_2O; **c**, **d** after the CO_2 hydrogenation reaction at 170 °C for over 100 h. **e** Methanol yield and **f** selectivity of Cu_2O nanocubes (NC) on ZnO, spherical Cu NPs on ZnO (NP), and the commercial reference catalyst (CR). Reprinted with permission from Ref. [189], Copyright 2022, American Chemical Society

effect and adsorption capacities of CO and H_2 during CO_2 hydrogenation. Melian-Cabrera et al. [194, 195] found the introduced noble metal such as Pd into Cu/ZnO or Cu/Zn/Al_2O_3 catalysts could efficiently enhance the H_2 activation, which could spill over the neighboring sites. Such a process results in the formation of a highly reduced catalyst surface, which could facilitate the catalytic hydrogenation behavior to produce methanol. These results clearly elucidate the importance of the metal nature by using Cu-based catalysts as examples in CO_2 hydrogenation to methanol.

4.2 The nature of the oxides

The oxides generally act as the support in CO_2 hydrogenation to methanol, which not only serve as the structural promoters, but also is the key active sites for CO_2 activation [196–212]. The commonly-used oxides in methanol synthesis reaction contain ZnO, ZrO_2, CeO_2, In_2O_3, and TiO_2 and so on, among which the most promising is ZnO [15, 161]. However, it is still controversial about the role of ZnO in this reaction. Behrens et al. thought the in situ formed CuZn(211) alloy from Cu interacting with defective ZnO sites as the active sites for methanol production [161], while the synergy of Cu and ZnO at the interface, i.e. the Cu–ZnO interface, was confirmed as the active sites in Kattel et al.'s report [168]. Both points were well verified by others in later studies. Moreover, the recent studies demonstrated In_2O_3 as a superb candidate support for methanol production from CO_2 hydrogenation [231, 232]. For instance, Cai et al. [231] used TCPP(Pd)@MIL-68(In) as precursors for the preparation of Pd/In_2O_3 catalysts, which exhibits extremely high performance for CO_2 hydrogenation, with a maximum methanol space–time yield of 81.1 g_{MeOH} h^{-1} $g_{Pd}{}^{-1}$ at 295 °C. Similar results were also observed by Frei et al. [232], who found that the $InNi_3$ patches formed on In_2O_3 surface with Ni loadings of no more than 10% can selectively drive CO_2 hydrogenation towards methanol over Ni/In_2O_3 catalysts.

In any cases, these clearly reveal the importance of oxides in CO_2 hydrogenation to methanol. Next, we will present comprehensive introductions of the particle size [196], the crystal phase [197–203], the morphology/crystal plane [174, 204–208], and composite [30, 209–212, 233–235] of the oxides in determining the catalysis of oxide-based catalysts for methanol production, respectively.

The particle sizes are always the crucial influencing factor in heterogeneous catalysis, not only restricted to metal NPs, but also extended to the oxide supports. Therefore, optimizing the particle size of the oxide supports is also proposed as an attractive approach for developing improved catalysts for methanol production. Chen et al. [196] prepared a series of ZnO-supported Au catalysts with the increase of ZnO particle size ranging from 22 to 103 nm but keeping constant Au particle size (Fig. 15a). The catalytic activity in CO_2 hydrogenation presents a volcano-type variation with increased ZnO particle size while the methanol selectivity increases continuously (Fig. 15a). The Au 4f XPS spectra coupling with EPR spectra (Fig. 15b and c) demonstrate that the volcano-type dependence could be related to the increasing surface oxygen vacancy concentrations with the ZnO particle size growing up that contributes to the MSIs together with the SMSI effects causing partial overgrowth of a ZnO_x layer, resulting in an increasing charge density on interfacial Au sites and their adsorption strength. Consequently, an optimum Au NP density supported on ZnO with moderate particle size exhibits the maximum methanol formation rate according to the Sabatier principle. The increasing methanol selectivity could arise from the differences of methanol formation and CO formation varying with the ZnO particle size by different optimum oxygen vacancy concentrations and electronic structures of the active sites.

The crystal phases of oxide support also significantly affect the interfacial catalysis in CO_2 hydrogenation to methanol, which has been frequently observed on ZrO_2 supports [197–202]. For Cu/ZrO_2-catalyzed methanol synthesis reaction, Samson et al. [199] found the tetrahedral phase ZrO_2 supported Cu catalyst was more active for methanol synthesis (Fig. 16a), which was associated with the complexes formed preferentially on t-ZrO_2 to build the Cu^+ cations and oxygen vacancies as acidic centers. Thus, the catalytic activity for methanol production increases with the t-ZrO_2 content increase. Similar

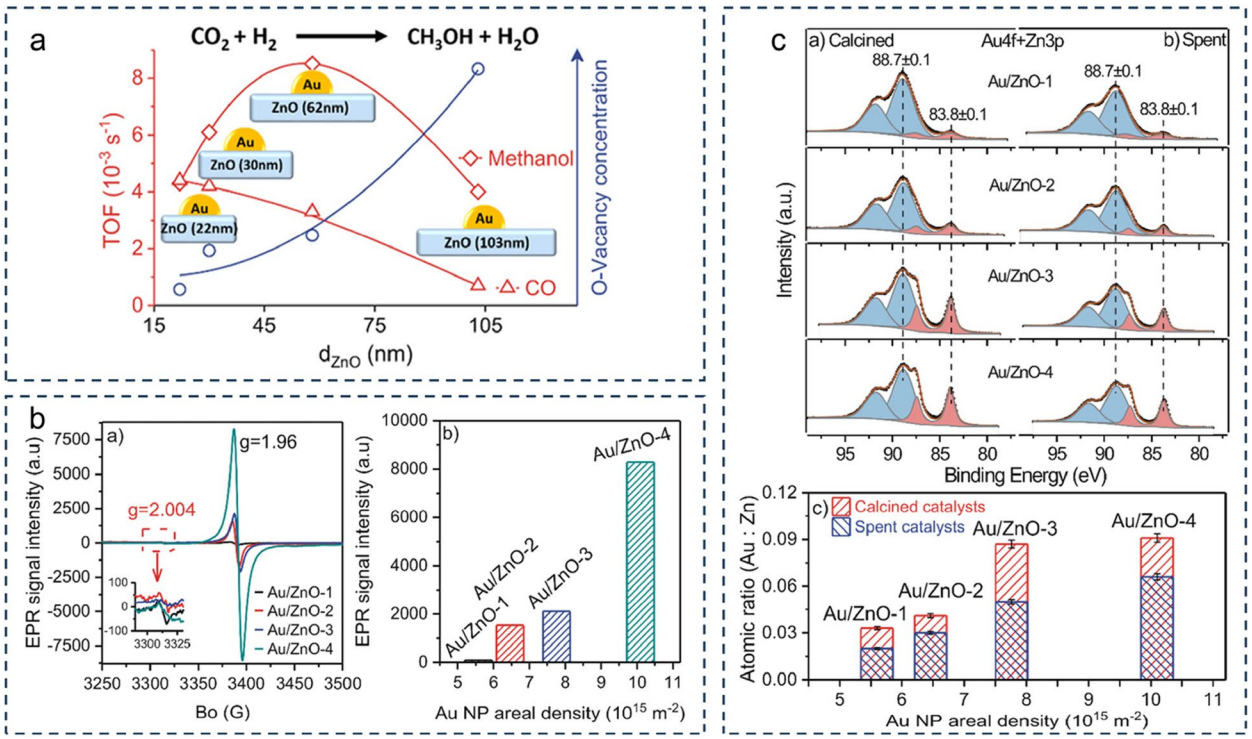

Fig. 15 (a) TOFs, product selectivity, and oxygen vacancy concentrations of the Au/ZnO catalysts varying with ZnO particle size increase. (b) EPR spectra collected after the reaction at high pressures at 240 °C in a CO_2/H_2 gas mixture and relative intensities of the O-vacancy signal (g = 1.96). (c) Au 4f XPS and Zn 3p XPS spectra of the Au/ZnO catalysts after calcination (calcined) and after reaction at high pressures at 240 °C in a CO_2/H_2 gas mixture (spent), and corresponding surface atomic Au:Zn ratios. Reprinted with permission from Ref. [196], Copyright 2021, American Chemical Society

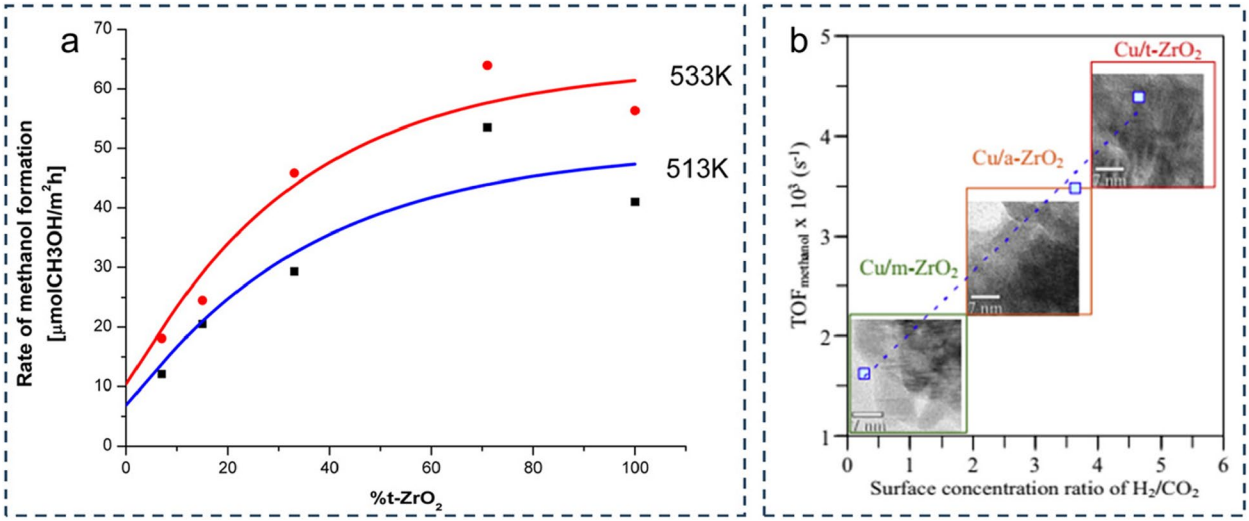

Fig. 16 **a** Methanol formation rate as a function of t-ZrO_2 content. **b** TOFs of various Cu/ZrO_2 catalysts varying with surface concentration ratio of H_2/CO_2. Reprinted with permission from Refs. [199] and [200], Copyright 2014 and 2016, American Chemical Society and Elsevier

results were also observed by Witoon et al. [200], who reported that Cu/t-ZrO_2 catalyst was more intrinsically active with the calculated TOF value on basis of surface copper sites ca 1.10–1.15 times and 1.62–3.59 times higher than Cu/a-ZrO_2 (amorphous) and Cu/m-ZrO_2 catalysts, respectively (Fig. 16b). Such a high TOF over Cu/t-ZrO_2 catalyst could be ascribed to a stronger Cu-ZrO_2 interaction and a higher surface concentration of hydrogenation atoms for CO_2 conversion.

In addition to the crystal phases, the exposed crystal planes of oxide support by tuning the morphologies play a crucial role in determining the catalytic performance [174, 204–208]. Taking ZnO as an example, Liao et al. [205] found the polarity of exposed crystal planes strongly affecting the Cu–ZnO interactions and thus results in different interfacial catalysis in CO_2 hydrogenation. They first prepared two types of ZnO supports, respectively platelike ZnO (p-ZnO) predominantly exposing polar (002) facets and rodlike ZnO (r-ZnO) predominantly exposing nonpolar (100) and (101) facets (Fig. 17a-d). A physically mixed method was employed to synthesize Cu–ZnO catalysts, whose selectivity in methanol synthesis was sensitive to ZnO morphology. A higher methanol selectivity over Cu/p-ZnO mixed with Al_2O_3 catalysts, affording a value of 71.6% at 280 °C, was observed (Fig. 17e), which was associated with stronger Cu–ZnO interactions occurring between Cu and p-ZnO support. This result clearly demonstrated the concept of morphology-dependent MSIs that are of importance in determining reaction selectivity for CO_2 hydrogenation.

The composite oxides acting as the support generally exhibit better catalytic performance in methanol synthesis from CO_2 hydrogenation than corresponding single component, which could be ascribed to diverse factors [30, 209–212]. Graciani et al. [16] found that the existence of TiO_2(110) can promote the formation of small wirelike ceria structures with stable Ce(III) and Ce(IV) states. Compared to CeO_x/Cu(111) model catalyst, the intrinsic activity for methanol production over Cu/CeO_x/TiO_2(110) was greatly enhanced with a TOF of 8.1 molecule per active site per second. Zhan et al. [210] prepared a quaternary Cu–ZnO-ZrO_2-TiO_2 catalyst by a coprecipitation method. They found that the addition of ZrO_2 and TiO_2 into Cu–ZnO catalyst can result in a decreased crystallite size for both CuO and ZnO that are beneficial for the increases of Cu surface area and the Cu–ZnO interaction, contributing to increased methanol yield in CO_2 hydrogenation. Similarly, Angelo et al. [211] demonstrated that, compared to CeO_2, the addition of ZrO_2 into Cu–ZnO-Al_2O_3 catalyst efficiently promoted the methanol production from CO_2 hydrogenation. Recently, Wang et al. [233] found that ZnO-ZrO_2 solid solution catalyst exhibits a high selectivity and stability for CO_2 hydrogenation to methanol. Using this as the support, Yan et al.'s group developed $ZnZrO_x$ solid solution supported Pd single atom [234] and an optimized integration of $ZnZrO_x$ solid solution and Pd supported on carbon nanotube [235] for enhanced methanol production from CO_2 hydrogenation.

In addition to the support, the oxides can also be supported on metal over inverse oxide/metal catalysts that sometimes exhibit enhanced interfacial reactivity compared to corresponding metal/oxide catalysts, which have been well verified in well-defined ZnO/Cu(111) and

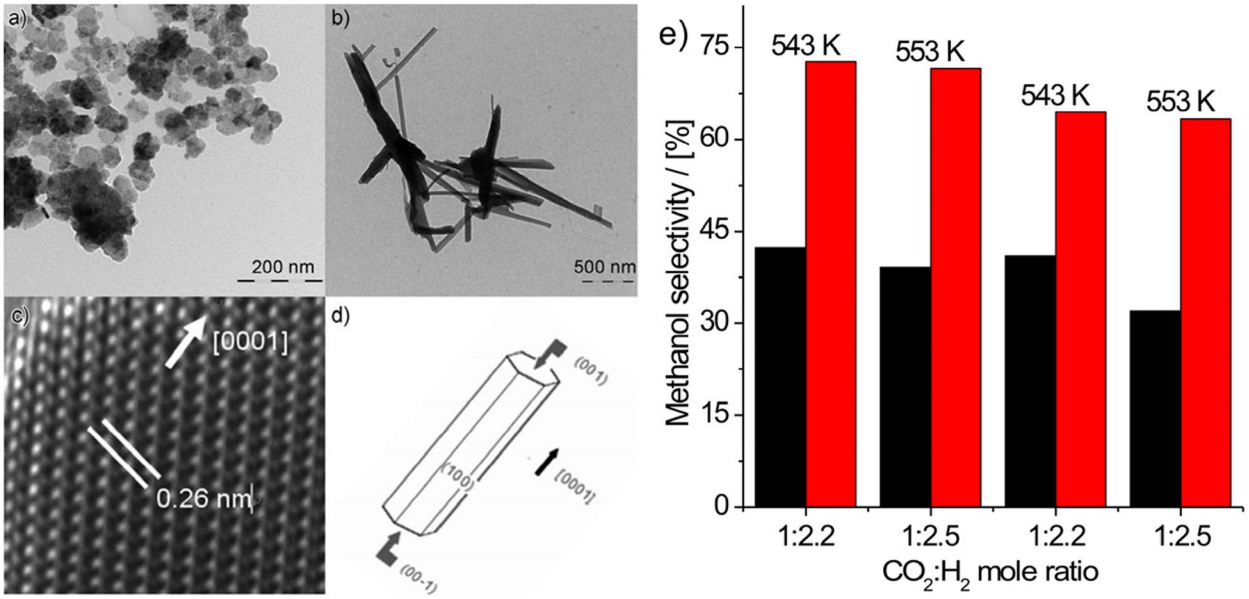

Fig. 17 TEM images of **a** ZnO plate particles and **b** ZnO nanorods. **c** HRTEM image of ZnO rod. **d** Crystallographic relationship between ZnO plate and rod. **e** Catalytic performance of ZnO plate and rod particles mixed with copper and alumina in the synthesis of methanol from hydrogenation of CO_2. Reprinted with permission from Ref. [205], Copyright 2011, Wiley–VCH Verlag GmbH & Co. KGaA, Weinheim and American Chemical Society

CeO_x/Cu(111) model catalysts for methanol synthesis [187, 213, 214]. Recently, this process was also experimentally demonstrated over a ZrO_2/Cu inverse configuration for CO_2 hydrogenation reported by Wu et al. [215]. An oxalate coprecipitation method was employed to prepare inverse ZrO_2/Cu catalysts with a tunable Zr/Cu ratio (Fig. 18a). The optimal activity in CO_2 hydrogenation was observed over inverse ZrO_2/Cu catalyst with a Zr/Cu ratio of 1:9, affording a mass-specific methanol formation rate of 524 g_{MeOH} kg_{cat}^{-1} h^{-1} at 220 °C (Fig. 18b), which is 3.3 times higher than that over traditional Cu/ZrO_2 catalyst (159 g_{MeOH} kg_{cat}^{-1} h^{-1}). Microscopic characterizations demonstrated that the formed ZrO_2 is partially reduced amorphous and exists in the form of islands with a particle size of 1–2 nm (Fig. 18a). In situ DRIFTS spectra showed that the formation and consumption of formate and methoxy intermediates are much faster over inverse ZrO_2/Cu catalysts than over Cu/ZrO_2 catalysts (Fig. 18c). Therefore, the excellent methanol formation rate over inverse ZrO_2/Cu configuration could be ascribed to the activation of CO_2 and hydrogenation of all the surface oxygenate intermediates proceeded easily.

The (S)MSIs, contributing to the methanol production from CO_2 hydrogenation, have also been frequently observed over metal/oxide catalysts [217–222]. Typical in Cu-based catalysts for CO_2 hydrogenation to methanol associated with the MSIs, Wang et al. [219] found the interactions at the Cu/CeO_2 interfaces are more efficient than those at the Cu/ZrO_2 interfaces, which could improve the dispersion of supported Cu species and the formation of surface oxygen vacancies, and consequently accelerate the methanol production from CO_2 hydrogenation via the formation of surface carbonates intermediates. For the SMSI effect, Zhang et al. [222] observed a size-dependent SMSIs in Pd/ZnO catalysts, in which the Pd NPs with larger sizes are more prone to be encapsulated by ZnO support during reducible conditions than those of smaller ones. This will lead to the different formation of Pd-ZnO interfaces and thus varied CO binding strength. Consequently, the Pd/ZnO catalysts with larger Pd particle sizes exhibit best catalytic activity and methanol selectivity that that with a Pd particle size of 1.6 nm.

5 Summary and outlook

To face the global warming and changing climate caused by CO_2 emission generated from the utilizations of nonrenewable fossil energies, the urgent issue in modern society is to reduce CO_2 content in the atmosphere. Catalytic CO_2 hydrogenation to value-added chemicals is regarded as a superior approach to address this issue, while this process is seriously limited by highly chemical inertia of CO_2 and complexly catalytic routes of CO_2 hydrogenation reaction. In this review, we summarized the recent progress of metal-oxide nanocatalysts for CO_2 hydrogenation to value-added C1 chemicals (CH_4/CO, FA/formate, and methanol) and revealed that the structures of metal-oxide interfaces were crucial in determining both the catalytic activity and the product selectivity.

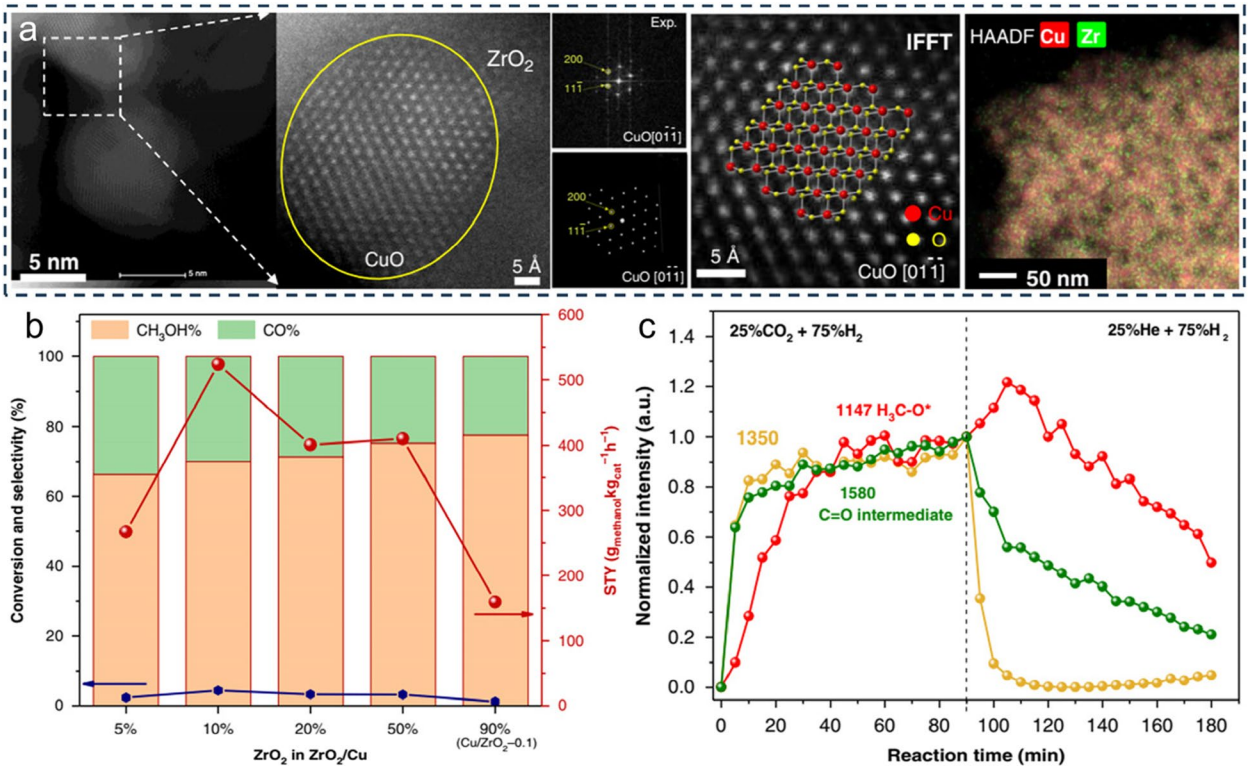

Fig. 18 **a** High-resolution HAADF-STEM images/FFT patterns with simulated results and the EDS elemental mapping of ZrO_2/Cu-0.1 catalyst. **b** CO_2 conversion, product selectivity and space time yield (STY) of methanol as a function of the percentage of ZrO_2 in the ZrO_2/Cu catalysts. **c** Normalized intensities of the typical surface species versus reaction time (first 90 min in 75% H_2/25% CO_2 atmosphere at 220 °C and the inlet was switched to 75% H_2/25% He at 90 min and maintained at the same temperature for another 90 min) over ZrO_2/Cu-0.2 catalyst. Reprinted with permission from Ref. [215], Copyright 2020, Nature Publishing Group

The various factors affecting the interfacial structures of metal-oxide nanocatalysts are presented, including the type, the particle size, the crystal plane/morphology, and the bimetal alloy of the metal NPs, the type, the particle size, the crystal phase, the crystal plane/morphology, and the composite of the oxides, and their (S)MSIs. By these studies, the interfacial catalysis of metal-oxide nanocatalysts in CO_2 hydrogenation is in depth elucidated and the key factors determining the reaction activity, product selectivity, and catalytic stability are efficiently unveiled, which provide the guides for the structural design of metal-oxide nanocatalysts with good activity and high selectivity in CO_2 conversion.

Nonetheless, the current studies are less comprehensive and the following points still need to be considered that will also offer challenging opportunities in the future research. Firstly, the interfacial structures are extremely complex with affected factors diversely, not limited to the summarized contents in this review. This will lead to the results reported in literature not wholly, giving an incomplete conclusion to the readers. Secondly, the interfacial numbers at atomic level are hardly counted due to the irregular shapes and random contacts between metals and oxides for powder catalysts, which are unbeneficial for comprehensive understanding the interfacial catalysis in CO_2 hydrogenation. Thirdly, the interfacial change transfer associated with the (S)MSIs is hardly supervised and quantitative. The current studies mostly employing spectroscopic characterizations such as XPS and in situ CO-DRIFTS only give an average electronic information of supported metal species to compare the charge transfer relatively. Due to the complexity of powder catalysts, the electronic information from non-interfacial sites can also be detected, which could bring about undesirable results. Fourth, an interfacial reconstruction could occur during reaction conditions, which may result in a wrong relationship between the probed ex situ structures and the catalytic performance, restricting the precise identification of the active site in CO_2 hydrogenation.

Currently, as the significant promotion of nanosynthesis technology as well as the continuous development of in situ characterizations, the design and corresponding detection of interfacial structures have been gradually improved to bring new opportunities for the studies of

interfacial catalysis of metal-oxide nanocatalysts in CO_2 hydrogenation. Considering the complex structures of powder catalysts, this study is still challenging and the development of efficient and operable approach is very impending. Oppositely, this also provides new opportunities for further study in the future. Totally, this is a research subject with both opportunities and challenges.

Acknowledgements
This work was financially supported by the National Natural Science Foundation of China (No. 21773212), the Jinhua Industrial Key Project (No. 20221080), and the self-designed scientific research project of Zhejiang Normal University (No. 2021ZS0602).

Author contributions
Z. Zhang supervised and wrote this project. Z. Wang assited with the writting and comment on the manuscript.

Funding
National Natural Science Foundation of China, 21773212, Zhenhua Zhang, Jinhua Industrial Key Project, 20221080, Zhenhua Zhang, self-designed scientific research project of Zhejiang Normal University, 2021ZS0602, Zhenhua Zhang.

Declarations

Competing interests
There are no conflicts to declare.

Received: 30 June 2023 Revised: 27 July 2023 Accepted: 23 August 2023
Published online: 12 October 2023

References

1. Wang W, Wang S, Ma X et al (2011) Recent advances in catalytic hydrogenation of carbon dioxide. Chem Soc Rev 40:3703–3727
2. Wang L, Chen W, Zhang D et al (2019) Surface strategies for catalytic CO_2 reduction: from two-dimensional materials to nanoclusters to single atoms. Chem Soc Rev 48:5310–5349
3. Knutson TR, Tuleya RE (2004) Impact of CO2-induced warming on simulated hurricane intensity and precipitation: sensitivity to the choice of climate model and convective parameterization. J Clim 17:3477-3495
4. Hansen J, Sato M, Ruedy R et al (2006) Global temperature change. Proc Natl Acad Sci U S A 103:14288
5. Appel AM, Bercaw JE, Bocarsly AB et al (2013) Frontiers, opportunities, and challenges in biochemical and chemical catalysis of CO_2 fixation. Chem Rev 113:6621–6658
6. Álvarez A, Bansode A, Urakawa A et al (2017) Challenges in the greener production of formates/formic acid, methanol, and DME by heterogeneously catalyzed CO_2 hydrogenation processes. Chem Rev 117:9804–9838
7. Zhou W, Cheng K, Kang J et al (2019) New horizon in C1 chemistry: breaking the selectivity limitation in transformation of syngas and hydrogenation of CO_2 into hydrocarbon chemicals and fuels. Chem Soc Rev 48:3193–3228
8. Xu D, Wang Y, Ding M et al (2021) Advances in higher alcohol synthesis from CO_2 hydrogenation. Chem 7:849–881
9. Gao P, Zhang L, Li S et al (2020) Novel heterogeneous catalysts for CO_2 hydrogenation to liquid fuels. ACS Cent Sci 6:1657–1670
10. Zhou Z, Gao P (2001) Direct carbon dioxide hydrogenation to produce bulk chemicals and liquid fuels via heterogeneous catalysis. Chin J Catal 43:2045–2056
11. Arakawa H, Aresta M, Armor JN et al (2001) Catalysis research of relevance to carbon management: progress, challenges, and opportunities. Chem Rev 101:953–996
12. Hua Z, Yang Y, Liu J (2023) Direct hydrogenation of carbon dioxide to value-added aromatics. Coord Chem Rev 478:214982
13. Kattel S, Liu P, Chen JG (2017) Tuning selectivity of CO_2 hydrogenation reactions at the metal/oxide interface. J Am Chem Soc 139:9739–9754
14. Khdary NH, Alayyar AS, Alsarhan LM et al (2022) Metal oxides as catalyst/supporter for CO_2 capture and conversion, review. Catalysts 12:300
15. BASF (1923) German Patents 415686, 441433, 462837
16. Graciani J, Mudiyanselage K, Xu F et al (2014) Highly active copper-ceria and copper-ceria-titania catalysts for methanol synthesis from CO_2. Science 345:546–550
17. Kattel S, Yu W, Yang X et al (2016) CO_2 hydrogenation over oxide-supported PtCo catalysts: the role of the oxide support in determining the product selectivity. Angew Chem Int Ed 55:7968–7973
18. Caparrós FJ, Soler L, Rossell MD et al (2018) Remarkable carbon dioxide hydrogenation to ethanol on a palladium/iron oxide single-atom catalyst. ChemCatChem 10:2365–2369
19. Yan Y, Wong RJ, Ma Z et al (2022) CO_2 hydrogenation to methanol on tungsten-doped Cu/CeO_2 catalysts. Appl Catal B: Environ 306:121098
20. Sha B, Wang Z-Q, Gong X-Q et al (2023) Synergistic promotions between CO_2 capture and in-situ conversion on Ni-CaO composite catalyst. Nat Commun 14:996
21. Yan B, Zhao B, Kattel S et al (2019) Tuning CO_2 hydrogenation selectivity via metal-oxide interfacial sites. J Catal 374:60–71
22. Parastaev A, Muravev V, Osta EH et al (2022) Breaking structure sensitivity in CO_2 hydrogenation by tuning metal-xide interfaces in supported cobalt nanoparticles. Nat Catal 5:1051–1060
23. Liao W, Tang C, Zheng H et al (2022) Tuning activity and selectivity of CO_2 hydrogenation via metal-oxide interfaces over ZnO-supported metal catalysts. J Catal 407:126–140
24. Liao W, Yue M, Chen J et al (2023) Decoupling the interfacial catalysis of CeO_2-supported Rh catalysts tuned by CeO_2 morphology and Rh particle size in CO_2 hydrogenation. ACS Catal 13:5767–5779
25. Lam E, Corral-Pérez JJ, Larmier K et al (2019) CO_2 hydrogenation on Cu/Al_2O_3: role of the metal/support interface in driving activity and selectivity of a bifunctional catalyst. Angew Chem Int Ed 58:13989–13996
26. Cao F, Song Z, Zhang Z et al (2021) Size-controlled synthesis of Pd nanocatalysts on defect-engineered CeO_2 for CO_2 hydrogenation. ACS Appl Mater Interfaces 13:24957–24965
27. Senanayake SD, Ramírez PJ, Waluyo I et al (2016) Hydrogenation of CO_2 to methanol on $CeO_x/Cu(111)$ and ZnO/Cu(111) catalysts: role of the metal-oxide interface and importance of Ce^{3+} sites. J Phys Chem C 120:1778–1784
28. Guo Y, Liu Z, Zhang F et al (2021) Modulation of the effective metal-support interactions for the selectivity of ceria supported noble metal nanoclusters in atmospheric CO_2 hydrogenation. ChemCatChem 13:874–881
29. Zhang S, Fan Q, Xia R et al (2020) CO_2 reduction: from homogeneous to heterogeneous electrocatalysis. Acc Chem Res 53:255–264
30. Aziz MAA, Jalil AA, Triwahyono S et al (2016) CO_2 methanation over heterogeneous catalysts: recent progress and future prospects. Green Chem 17:2647–2663
31. Miao B, Ma SSK, Wang X et al (2016) Catalysis mechanisms of CO_2 and CO methanation. Catal Sci Techno 6:4048–4058
32. Ashok J, Pati S, Hongmanorom P et al (2020) A review of recent catalyst advances in CO_2 methanation processes. Catal Today 356:471–489
33. Chen S, Abdel-Mageed AM (2023) Methanation reactions for chemical storage and purification of hydrogen: overview and structurereactivity correlations in supported metals. Int J Hydrogen Energy. https://doi.org/10.1016/j.ijhydene.2022.12.196
34. Rostrup-Nielsen, JR (1984) Catalytic steam reforming, vol. 5. Catal Sci Technol 5:1-117
35. Dagle RA, Wang Y, Xia G-G et al (2007) Selective CO methanation catalysts for fuel processing applications. Appl Catal A: Gen 326:213–218
36. Vogt C, Monai M, Kramer GJ et al (2019) The renaissance of the Sabatier reaction and its applications on earth and in space. Nat Catal 2:188–197
37. Tian D, Liu Z, Li D et al (2013) Bimetallic Ni-Fe total-methanation catalyst for the production of substitute natural gas under high pressure. Fuel 104:224–229
38. Xiang Y, Kruse N (2016) Tuning the catalytic CO hydrogenation to straight and long-chain aldehydes/alcohols and olefins/paraffins. Nat Commun 7:13058
39. Shi Z, Yang H, Gao P et al (2018) Effect of alkali metals on the performance of $CoCu/TiO_2$ catalysts for CO_2 hydrogenation to long-chain hydrocarbons. Chin J Catal 39:1294–1302

40. Zhang Z, Shen C, Sun K et al (2022) Advances in studies of the structural effects of supported Ni catalysts for CO_2 hydrogenation: from nanoparticle to single atom catalyst. J Mater Chem A 10:5792–5812
41. Rui N, Zhang X, Zhang F et al (2021) Highly active Ni/CeO_2 catalyst for CO_2 methanation: preparation and characterization. Appl Catal B: Environ 282:119581
42. Gao M, Zhang J, Zhu P et al (2022) Unveiling the origin of alkali metal promotion in CO_2 methanation over Ru/ZrO_2. Appl Catal B: Environ 314:121476
43. Xu J, Li L, Pan J et al. (2022) Boosting the catalytic performance of CuO_x in CO_2 hydrogenation by incorporating CeO_2 promoters. Adv Sustainable Syst 6:2100439
44. Li Y, Men Y, Liu S et al (2021) Remarkably efficient and stable Ni/Y_2O_3 catalysts for CO_2 methanation: effect of citric acid addition. Appl Catal B: Environ 293:120206
45. Moiolia E, Züttel A (2020) A model-based comparison of Ru and Ni catalysts for the Sabatier reaction. Sustain Energy Fuels 4:1396–1408
46. Martin NM, Velin P, Skoglundh M et al (2017) Catalytic hydrogenation of CO_2 to methane over supported Pd, Rh and Ni catalysts. Catal Sci Technol 7:1086–1094
47. Quindimil A, De-La-Torre U, Pereda-Ayo B et al (2020) Effect of metal loading on the CO_2 methanation: a comparison between alumina supported Ni and Ru catalysts. Catal Today 356:419–432
48. Panagiotopoulou P (2017) Hydrogenation of CO_2 over supported noble metal catalysts. Appl Catal A: Gen 542:63–70
49. Varun Y, Sreedhar I, Singh SA (2020) Highly stable M/NiO-MgO (M = Co, Cu and Fe) catalysts towards CO_2 methanation. Int J Hydrogen Energy 45:28716–28731
50. Martin NM, Hemmingsson F, Schaefer A et al (2019) Structure-function relationship for CO_2 methanation over ceria supported Rh and Ni catalysts under atmospheric pressure conditions. Catal Sci Technol 9:1644–1653
51. Kwak JH, Kovarik L, Szanyi J et al (2013) CO_2 reduction on supported Ru/Al_2O_3 catalysts: cluster size dependence of product selectivity. ACS Catal 3:2449–2455
52. Hao Z, Shen J, Lin S et al (2021) Decoupling the effect of Ni particle size and surface oxygen deficiencies in CO_2 methanation over ceria supported Ni. Appl Catal B: Environ 286:119922
53. Lin L, Gerlak CA, Liu C et al (2021) Effect of Ni particle size on the production of renewable methane from CO_2 over Ni/CeO_2 catalyst. J Energy Chem 61:602–611
54. Feng K, Tian J, Guo M et al (2021) Experimentally unveiling the origin of tunable selectivity for CO_2 hydrogenation over Ni-based catalysts. Appl Catal B: Environ 292:120191
55. Guo Y, Mei S, Yuan K et al (2018) Low-temperature CO_2 methanation over CeO_2-supported Ru single atoms, nanoclusters, and nanoparticles competitively tuned by strong metal-support interactions and H-spillover effect. ACS Catal 8:6203–6215
56. Wang D, Yuan Z, Wu X et al (2023) Ni single atoms confined in nitrogen-doped carbon nanotubes for active and selective hydrogenation of CO_2 to CO. ACS Catal 13:7132–7138
57. Zheng H, Liao W, Ding J et al (2022) Unveiling the key factors in determining the activity and selectivity of CO_2 hydrogenation over Ni/CeO_2 catalysts. ACS Catal 12:15451–15462
58. Guo J, Wang Z, Li J et al (2022) In-Ni intermetallic compounds derived from layered double hydroxides as efficient catalysts toward the reverse water gas shift reaction. ACS Catal 12:4026–4036
59. Wang Y, Feng K, Tian J et al (2022) Atomically dispersed Zn-stabilized $Ni^{\delta+}$ enabling tunable selectivity for CO_2 hydrogenation. Chemsuschem 15:e202102439
60. Mutz B, Belimov M, Wang W et al (2017) Potential of an alumina-supported Ni_3Fe catalyst in the methanation of CO_2: impact of alloy formation on activity and stability. ACS Catal 7:6802–6814
61. Lu H, Yang X, Gao G et al (2016) Metal (Fe Co, Ce or La) doped nickel catalyst supported on ZrO2 modified mesoporous clays for CO and CO2 methanation. Fuel 183:335–344
62. Moghaddam SV, Rezaei M, Meshkani F et al (2018) Carbon dioxide methanation over Ni-M/Al_2O_3 (M: Fe, CO, Zr, La and Cu) catalysts synthesized using the one-pot sol-gel synthesis method. Int J Hydrogen Energy 43:16522–16533
63. Luo L, Wang M, Cui Y et al (2020) Surface iron species in palladium-iron intermetallic nanocrystals that promote and stabilize CO_2 methanation. Angew Chem Int Ed 59:14434–14442
64. Arandiyan H, Wang Y, Scott J et al (2018) In situ exsolution of bimetallic Rh-Ni nanoalloys: a highly efficient catalyst for CO_2 methanation. ACS Appl Mater Interfaces 10:16352–16357
65. Navarro JC, Centeno MA, Laguna OH et al (2020) Ru-Ni/$MgAl_2O_4$ structured catalyst for CO_2 methanation. Renew Energy 161:120–132
66. Díez-Ramírez J, Sánchez P, Kyriakou V et al (2017) Effect of support nature on the cobalt-catalyzed CO_2 hydrogenation. J CO_2 Util 21:562–571
67. Tada S, Shimizu T, Kameyama H et al (2012) Ni/CeO_2 catalysts with high CO_2 methanation activity and high CH_4 selectivity at low temperatures. Int J Hydrogen Energy 7:5527–5531
68. Jiang Y, Lang J, Wu X et al (2020) Electronic structure modulating for supported Rh catalysts toward CO_2 methanation. Catal Today 356:570–578
69. Dreyer JAH, Li P, Zhang L et al (2017) Influence of the oxide support reducibility on the CO_2 methanation over Ru-based catalysts. Appl Catal B: Environ 219:715–726
70. Italiano C, Llorca J, Pino L et al (2020) CO and CO_2 methanation over Ni catalysts supported on CeO_2, $Al2O_3$ and Y_2O_3 oxides. Appl Catal B: Environ 264:118494
71. Ricca A, Truda L, Palma V (2019) Study of the role of chemical support and structured carrier on the CO_2 methanation reaction. Chem Eng J 377:120461
72. Wang F, He S, Chen H et al (2016) Active site dependent reaction mechanism over Ru/CeO_2 catalyst toward CO_2 methanation. J Am Chem Soc 138:6298–6305
73. Wang F, Li C, Zhang X et al (2015) Catalytic behavior of supported Ru nanoparticles on the 100}, {110}, and {111 facet of CeO2. J Catal 329:177–186
74. Jomjaree T, Sintuya P, Srifa A et al (2021) Catalytic performance of Ni catalysts supported on CeO_2 with different morphologies for low-temperature CO_2 methanation. Catal Today 375:234–244
75. Xie F, Xu S, Deng L et al (2020) CO_2 hydrogenation on Co/$CeO_{2-\delta}$ catalyst: morphology effect from CeO_2 support. Int J Hydrogen Energ 45:26938–26952
76. Xie Y, Chen J, Wu X et al (2022) Frustrated lewis pairs boosting low-temperature CO_2 methanation performance over Ni/CeO_2 nanocatalysts. ACS Catal 12:10587–10602
77. Bian Z, Chan Y, Yu Y et al (2020) Morphology dependence of catalytic properties of Ni/CeO_2 for CO_2 methanation: a kinetic and mechanism study. Catal Today 347:31–38
78. Yang B, Wang Y, Li L et al (2022) Probing the morphological effects of ReO_x/CeO_2 catalysts on the CO_2 hydrogenation reaction. Catal Sci Technol 12:1159–1172
79. Chai S, Men Y, Wang J et al (2019) Boosting CO_2 methanation activity on Ru/TiO_2 catalysts by exposing (001) facets of anatase TiO_2. J CO_2 Util 33:242–252
80. Sakpal T, Lefferts L et al (2018) Structure-dependent activity of CeO_2 supported Ru catalysts for CO_2 methanation. J Catal 367:171–180
81. Ussa Aldana PA, Ocampo F, Kobl K et al (2013) Catalytic CO_2 valorization into CH_4 on Ni-based ceria-zirconia. reaction mechanism by operando IR spectroscopy. Catal Today 215:201–207
82. Pan Q, Peng J, Sun T et al (2014) CO_2 methanation on Ni/$Ce_{0.5}Zr_{0.5}O_2$ catalysts for the production of synthetic natural gas. Fuel Process Technol 123:166–171
83. Ocampo F, Louis B, Kiwi-Minsker L et al (2011) Effect of Ce/Zr composition and noble metal promotion on nickel based $Ce_xZr_{1-x}O_2$ catalysts for carbon dioxide methanation. Appl Catal A: Gen 392:36–44
84. Cai M, Wen J, Chu W et al (2011) Methanation of carbon dioxide on Ni/ZrO_2-Al_2O_3 catalysts: effects of ZrO_2 promoter and preparation method of novel ZrO_2-Al_2O_3 carrier. J Nat Gas Chem 20:318–324
85. Xu S, Xie F, Xie H et al (2019) Effect of structure and composition on the CO_2 hydrogenation properties over bimodal mesoporous CeCo composite catalyst. Chem Eng J 375:122023
86. Abate S, Mebrahtu C, Giglio E et al (2016) Catalytic performance of γ-Al_2O_3-ZrO_2-TiO_2-CeO_2 composite oxide supported Ni-based for CO2 Methanation. Ind Eng Chem Res 55:4451–4460

87. Liu H, Zou X, Wang X et al (2012) Effect of CeO_2 addition on Ni/Al_2O_3 catalysts for methanation of carbon dioxide with hydrogen. J Nat Gas Chem 21:703–707
88. Zeng Y, Ma H, Zhang H et al (2014) Highly efficient $NiAl_2O_4$-free $Ni/c\text{-}Al_2O_3$ catalysts prepared by solution combustion method for CO methanation. Fuel 137:155–163
89. Parastaev A, Muravev V, Osta EH et al (2020) Boosting CO_2 hydrogenation via size-dependent metal-support interactions in cobalt/ceria-based catalysts. Nat Catal 3:526–533
90. Cárdenas-Arenas A, Quindimil A, Davó-Quinonero A et al (2020) Design of active sites in Ni/CeO_2 catalysts for the methanation of CO_2: tailoring the $Ni\text{-}CeO_2$ contact. Appl Mater Today 19:100591
91. Chen S, Abdel-Mageed AM, Dyballa M et al (2020) Raising the CO_x methanation activity of a $Ru/\gamma\text{-}Al_2O_3$ catalyst by activated modification of metal-support interactions. Angew Chem Int Ed 59:22763–22770
92. Zhang Y, Yan W, Qi H et al (2022) Strong metal-support interaction of Ru on TiO_2 derived from the Co-reduction mechanism of $Ru_xTi_{1-x}O_2$ interphase. ACS Catal 12:1697–1705
93. Xin H, Lin L, Li R et al (2022) Overturning CO_2 hydrogenation selectivity with high activity via reaction-induced strong metal-support interactions. J Am Chem Soc 144:4874–4882
94. Li S, Xu Y, Chen Y et al (2017) Tuning the selectivity of catalytic carbon dioxide hydrogenation over iridium/cerium oxide catalysts with a strong metal-support interaction. Angew Chem Int Ed 56:10761–10765
95. Lin L, Liu J, Liu X et al (2021) Reversing sintering effect of Ni particles on $\gamma\text{-}Mo_2N$ via strong metal support interaction. Nat Commun 12:6978
96. Du Y, Qin C, Xu Y et al Ni nanoparticles dispersed on oxygen vacancies-rich CeO_2 nanoplates for enhanced low-temperature CO_2 methanation performance. Chem Eng J 418:129402
97. Wulff G (1901) On the question of speed of growth and dissolution of crystal surfaces. Z Kristallogr 34:449–530
98. Huang W (2016) Oxide nanocrystal model catalysts. Acc Chem Res 49:520–527
99. Chen S, Xiong F, Huang W (2019) Surface chemistry and catalysis of oxide model catalysts from single crystals to nanocrystals. Surf Sci Rep 74:100471
100. Zhang Z, Wang S-S, Song R et al (2017) The most active Cu facet for low-temperature water gas shift reaction. Nat Commun 8:488
101. Zhang Z, Song R, Yu Z et al (2019) Crystal-plane effect of Cu_2O templates on compositions, structures and catalytic performance of Ag/Cu_2O nanocomposites. CrystEngComm 21:2002–2008
102. Zhang Z, Wu H, Yu Z et al (2019) Site-resolved Cu_2O catalysis in the oxidation of CO. Angew Chem Int Ed 58:4276–4280
103. Yu Z, Zhang Z, Zhang Y et al (2020) Titania morphology-dependent catalysis of CuO_x/TiO_2 catalysts in CO oxidation and water gas shift reactions. ChemCatChem 12:3679–3686
104. Gao Y, Zhang Z, Li Z et al (2020) Understanding morphology-dependent $CuO_x\text{-}CeO_2$ interactions from the very beginning. Chin J Catal 41:1006–1016
105. Zhang Z, Wang Z-Q, Li Z et al (2020) Metal-free ceria catalysis for selective hydrogenation of crotonaldehyde. ACS Catal 10:14560–14566
106. Zhang Z, Zhang J, Jia A-P et al (2020) Morphology-dependent CO reduction kinetics and surface copper species evolution of Cu_2O nanocrystals. J Phys Chem C 124:21568–21576
107. Zhang Z, Chen X, Kang J et al (2021) The active sites of Cu-ZnO catalysts for water gas shift and CO hydrogenation reactions. Nat Commun 12:4331
108. Wen Y, Huang Q, Zhang Z et al (2022) Morphology-dependent catalysis of CeO_2-based nanocrystal model catalysts. Chin J Chem 40:1856–1866
109. Wen Y, Xia L, Zhang J et al (2022) Tailoring $Ir\text{-}FeO_x$ interactions and catalytic performance in preferential oxidation of CO in H_2 via the morphology engineering of anatase TiO_2 over $Ir\text{-}FeOx/TiO_2$ catalysts. Mol Catal 528:112524
110. Zhang Z, Fan L, Liao W et al (2022) Structure sensitivity of CuO in CO oxidation over $CeO_2\text{-}CuO/Cu_2O$ catalysts. J Catal 405:333–345
111. Zhang Z, You R, Huang W (2022) Cu_2O nanocrystal model catalysts. Chin J Chem 40:846–855
112. Li D, Chen S, You R et al (2018) Titania-morphology-dependent dual-perimeter-sites catalysis by Au/TiO_2 catalysts in low-temperature CO oxidation. J Catal 368:163–171
113. Li D, You R, Yang M et al (2019) Morphology-dependent evolutions of sizes, structures, and catalytic activity of Au nanoparticles on anatase TiO_2 nanocrystals. J Phys Chem C 123:10367–10376
114. Yang M, Zhang J, Cao Y et al (2018) Facet sensitivity of capping ligand-free Ag crystals in CO_2 electrochemical reduction to CO. ChemCatChem 10:5128–5134
115. Jia A, Zhang Y, Song T et al (2021) Crystal-plane effects of anatase TiO_2 on the selective hydrogenation of crotonaldehyde over Ir/TiO_2 catalysts. J Catal 395:10–22
116. Cao T, You R, Li Z et al (2020) Morphology-dependent CeO_2 catalysis in acetylene semihydrogenation reaction. Appl Sur Sci 501:144120
117. Li Y, Zhang Y, Qian K et al (2022) Metal-support interactions in metal/oxide catalysts and oxide-metal interactions in oxide/metal inverse catalysts. ACS Catal 12:1268–1287
118. Zhang Y, Liu J-X, Qian K et al (2021) Structure sensitivity of $Au\text{-}TiO_2$ strong metal-support interactions. Angew Chem Int Ed 60:12074–12081
119. Matsubu J, Zhang S, DeRita L et al (2017) Adsorbate-mediated strong metal-support interactions in oxide-supported Rh catalysts. Nat Chem 9:120–127
120. Chen S, Abdel-Mageed AM, Li M et al (2021) Electronic metal-support interactions and their promotional effect on CO_2 methanation on Ru/ZrO_2 catalysts. J Catal 400:407–420
121. Reutemann W, Kieczka H (2000) Formic acid. In ullmann's encyclopedia of industrial chemistry. Wiley-VCH Verlag GmbH & Co. KGaA, Weinheim
122. Gunasekar GH, Park K, Jung K-D et al (2016) Recent developments in the catalytic hydrogenation of CO_2 to formic acid/formate using heterogeneous catalysts. Inorg Chem Front 3:882–895
123. Wang W, Niu M, Hou Y et al (2014) Catalytic conversion of biomass-derived carbohydrates to formic acid using molecular oxygen. Green Chem 16:2614–2618
124. Xu J, Zhang H, Zhao Y et al (2014) Heteropolyanion-based ionic liquids catalysed conversion of cellulose into formic acid without any additives. Green Chem 16:4931–4935
125. Enthaler S, Langermann JV, Schmidt T (2010) Carbon dioxide and formic acid-the couple for environmental-friendly hydrogen storage? Energy Environ Sci 3:1207–1217
126. Mellmann D, Sponholz P, Junge H et al (2016) Formic acid as a hydrogen storage material-development of homogeneous catalysts for selective hydrogen release. Chem Soc Rev 45:3954–3988
127. Yan N, Philippot K (2018) Transformation of CO_2 by using nanoscale metal catalysts: cases studies on the formation of formic acid and dimethylether. Curr Opin Chem Eng 20:86–92
128. Sun R, Liao Y, Bai ST et al (2021) Heterogeneous catalysts for CO_2 hydrogenation to formic acid/formate: from nanoscale to single atom. Energy Environ Sci 14:1247–1285
129. Verma P, Zhang S, Song S et al (2021) Recent strategies for enhancing the catalytic activity of CO_2 hydrogenation to formate/formic acid over Pd-based catalyst. J CO_2 Util 54:101765
130. Wang WH, Hull JF, Muckerman JT et al (2012) Second-coordination-sphere and electronic effects enhance iridium(iii)-catalyzed homogeneous hydrogenation of carbon dioxide in water near ambient temperature and pressure. Energ Environ Sci 5:7923–7926
131. Huff CA, Sanford MS (2013) Catalytic CO_2 hydrogenation to formate by a ruthenium pincer complex. ACS Catal 3:2412–2416
132. Hutschka F, Dedieu A, Eichberger M et al (1997) Mechanistic aspects of the rhodium-catalyzed hydrogenation of CO_2 to formic acid a theoretical and kinetic study. J Am Chem Soc 119:4432–4443
133. Su J, Yang L, Lu M et al (2015) Highly efficient hydrogen storage system based on ammonium bicarbonate/formate redox equilibrium over palladium nanocatalysts. Chemsuschem 8:813–816
134. Sun Q, Chen BWJ, Wang N et al (2020) Zeolite-encaged Pd-Mn nanocatalysts for CO_2 hydrogenation and formic acid dehydrogenation. Angew Chem Int Ed 59:20183–20191
135. Mori K, Sano T, Kobayashi H et al (2018) Surface engineering of a supported PdAg catalyst for hydrogenation of CO_2 to formic acid: elucidating the active Pd atoms in alloy nanoparticles. J Am Chem Soc 140:8902–8909
136. Zhang J, Liao W, Zheng H et al (2022) Morphology-engineered highly active and stable Pd/TiO_2 catalysts for CO_2 hydrogenation into formate. J Catal 405:152–163
137. Pandey PH, Pawar HS (2020) Cu dispersed TiO_2 catalyst for direct hydrogenation of carbon dioxide into formic acid. J CO_2 Util 41:101267

138. Liu Q, Yang X, Li L et al (2017) Direct catalytic hydrogenation of CO_2 to formate over a schiff-base-mediated gold nanocatalyst. Nat Commun 8:1407
139. Mori K, Taga T, Yamashita H (2017) Isolated single-atomic Ru catalyst bound on a layered double hydroxide for hydrogenation of CO_2 to formic acid. ACS Catal 7:3147–3151
140. Fu X-P, Peres L, Esvan J et al (2021) An air-stable, reusable Ni@$Ni(OH)_2$ nanocatalyst for CO_2/bicarbonate hydrogenation to formate. Nanoscale 13:8931–8939
141. Wu B, Yu X, Huang M et al (2022) Rh single atoms embedded in CeO_2 nanostructure boost CO_2 hydrogenation to HCOOH. Chin J Chem Eng 43:62–69
142. Zhang Z, Zhang L, Yao S et al (2019) Support-dependent rate-determining step of CO_2 hydrogenation to formic acid on metal oxide supported Pd catalysts. J Catal 376:57–67
143. Zhang Z, Zhang L, Hülsey MJ et al (2019) Zirconia phase effect in Pd/ZrO_2 catalyzed CO_2 hydrogenation into formate. Mol Catal 475:110461
144. Zhang J, Fan L, Zhao F et al (2020) Zinc oxide morphology-dependent Pd/ZnO catalysis in base-free CO_2 hydrogenation into formic acid. ChemCatChem 12:5540–5547
145. Fan L, Zhang J, Ma K et al (2021) Ceria morphology-dependent Pd-CeO_2 interaction and catalysis in CO_2 hydrogenation into formate. J Catal 397:116–127
146. Shao X, Miao X, Zhang T et al (2020) Pd nanoparticles supported on N- and P-Co-doped carbon as catalysts for reversible formate-based chemical hydrogen storage. ACS Appl Nano Mater 3:9209–9217
147. Zhang Z, Song R, Cao T et al (2016) Morphology-dependent structures and catalytic performances of Au nanostructures on Cu_2O nanocrystals synthesized by galvanic replacement reaction. J Energy Chem 25:1086–1091
148. Zhang Z, Cao T, Luo L et al (2016) Au-Cu alloy formation on cubic Cu_2O nanocrystals at ambient temperature and their catalytic performance. ChemNanoMat 2:861–865
149. Nguyen LTM, Park H, Banu M et al (2015) Catalytic CO_2 hydrogenation to formic acid over carbon nanotube-graphene supported PdNi alloy catalysts. RSC Adv 5:105560–105566
150. Masuda S, Mori K, Futamura Y et al (2018) PdAg nanoparticles supported on functionalized mesoporous carbon: promotional effect of surface amine groups in reversible hydrogen delivery/storage mediated by formic acid/CO_2. ACS Catal 8:2277–2285
151. Masuda S, Mori K, Kuwahara Y et al (2019) PdAg nanoparticles supported on resorcinolformaldehyde polymers containing amine groups: the promotional effect of phenylamine moieties on CO_2 transformation to formic acid. J Mater Chem A 7:16356–16363
152. Kuwahara Y, Fujie Y, Mihogi T et al (2020) Hollow mesoporous organosilica spheres encapsulating PdAg nanoparticles and poly(ethyleneimine) as reusable catalysts for CO_2 hydrogenation to formate. ACS Catal 10:6356–6366
153. Yang G, Kuwahara Y, Mori K et al (2021) Pd-Cu alloy nanoparticles confined within mesoporous hollow carbon spheres for the hydrogenation of CO_2 to formate. J Phys Chem C 125:3961–3971
154. Xu L, Cui T, Zhu J et al (2021) PdAg alloy nanoparticles immobilized on functionalized MIL-101-NH_2: effect of organic amines on hydrogenation of carbon dioxide into formic acid. New J Chem 45:6293–6300
155. Wang Z, Ren D, He Y et al (2023) Tailoring electronic properties and atom utilizations of the Pd species supported on anatase TiO_2{101} for efficient CO_2 hydrogenation to formic acid. ACS Catal 13:10056–10064
156. Lee JH, Ryu J, Kim JY et al (2014) Carbon dioxide mediated, reversible chemical hydrogen storage using a Pd nanocatalyst supported on mesoporous graphitic carbon nitride. J Mater Chem A 2:9490
157. Wang FN, Xu JM, Shao XZ et al (2016) Palladium on nitrogen-doped mesoporous carbon: a bifunctional catalyst for formate-based carbon-neutral hydrogen storage. Chemsuschem 9:246–251
158. Mondelli C, Puértolas B, Ackermann M et al (2018) Enhanced base-free formic acid production from CO_2 on Pd/g-C_3N_4 by tuning of the carrier defects. Chemsuschem 11:2859–2869
159. Olah GA, Goeppert A, Prakash GK (2009) Chemical recycling of carbon dioxide to methanol and DME: from greenhouse gas to renewable, environmentally carbon neutral fuels and synthetic hydrocarbons. J Org Chem 74:487–498
160. Ma J, Sun NN, Zhang XL et al (2009) A short review of catalysis for CO_2 conversion. Catal Today 148:221–231
161. Behrens M, Studt F, Kasatkin I et al (2012) The active site of methanol synthesis over Cu/ZnO/Al_2O_3. Ind Catal Sci 336:893–897
162. Bai S-T, Smet GD, Liao Y et al (2021) Homogeneous and heterogeneous catalysts for hydrogenation of CO_2 to methanol under mild conditions. Chem Soc Rev 50:4259–4298
163. Dubois J-L, Sayama K, Arakawa H (1992) Conversion of CO_2 to dimethylether and methanol over hybrid catalysts. Chem Lett 21:1115–1118
164. Chen W-H, Lin B-J, Lee H-M et al (2012) One-step synthesis of dimethyl ether from the gas mixture containing CO_2 with high space velocity. Appl Energy 98:92–101
165. Centi G, Perathoner S (2009) Opportunities and prospects in the chemical recycling of carbon dioxide to fuels. Catal Today 148:191–205
166. Saeidi S, Amin NAS, Rahimpour MR (2014) Hydrogenation of CO_2 to value-added products-a review and potential future developments. J CO_2 Util 5:66–81
167. Ojelade OA, Zaman SF (2020) A review on Pd based catalysts for CO_2 hydrogenation to methanol: in-depth activity and DRIFTS mechanistic study. Catal Surv Asia 24:11–37
168. Kattel S, Ramírez PJ, Chen JG et al (2017) Active sites for CO_2 hydrogenation to methanol on Cu/ZnO catalysts. Science 355:1296–1299
169. Laudenschleger D, Ruland H, Muhler M (2020) Identifying the nature of the active sites in methanol synthesis over Cu/ZnO/Al_2O_3 catalysts. Nat Commun 11:3898
170. Zhu J, Su Y, Chai J et al (2020) Mechanism and nature of active sites for methanol synthesis from CO/CO_2 on Cu/CeO_2. ACS Catal 10:11532–11544
171. Cao A, Wang Z, Li H et al (2021) New insights on CO and CO_2 hydrogenation for methanol synthesis: the key role of adsorbate-adsorbate interactions on Cu and the highly active MgO-Cu interface. J Catal 400:325–331
172. Liu X, Luo J, Wang H et al (2022) In situ spectroscopic characterization and theoretical calculations identify partially reduced ZnO_{1-x}/Cu interfaces for methanol synthesis from CO_2. Angew Chem Int Ed 61:e2022023
173. Yang X, Kattel S, Senanayake SD et al (2015) Low pressure CO_2 hydrogenation to methanol over gold nanoparticles activated on a CeO_x/TiO_2 interface. J Am Chem Soc 137:10104–10107
174. Jiang F, Wang S, Liu B et al (2020) Insights into the influence of CeO_2 crystal facet on CO_2 hydrogenation to methanol over Pd/CeO_2 catalysts. ACS Catal 10:11493–11509
175. Kuld S, Thorhauge M, Falsig H et al (2016) Quantifying the promotion of Cu catalysts by ZnO for methanol synthesis. Science 352:969–974
176. Wang J, Meeprasert J, Han Z et al (2022) Highly dispersed Cd cluster supported on TiO_2 as an efficient catalyst for CO_2 hydrogenation to methanol. Chin J Catal 43:761–770
177. Tada S, Watanabe F, Kiyota K et al (2017) Ag addition to CuO-ZrO_2 catalysts promotes methanol synthesis via CO_2 hydrogenation. J Catal 351:107–118
178. Wu W, Wang Y, Luo L et al (2022) CO_2 hydrogenation over copper/ZnO single-atom catalysts: water-promoted transient synthesis of methanol. Angew Chem Int Ed 61:e202213024
179. Chen S, Abdel-Mageed AM, Hauble A et al (2021) Performance of Au/ZnO catalysts in CO_2 reduction to methanol: varying the Au loading / Au particle size. Appl Catal A: Gen 624:118318
180. Rui N, Wan Z, Sun K et al (2017) CO_2 hydrogenation to methanol over Pd/In_2O_3: effects of Pd and oxygen vacancy. Appl Catal B: Environ 218:488–497
181. Karelovic A, Ruiz P (2015) The role of copper particle size in low pressure methanol synthesis via CO_2 hydrogenation over Cu/ZnO catalysts. Catal Sci Technol 5:869–881
182. Hartadi Y, Widmann D, Jrgen Behm R (2015) CO_2 hydrogenation to methanol on supported Au catalysts under moderate reaction conditions: support and particle size effects. Chemsuschem 8:456–465
183. Jiang F, Yang Y, Wang L et al (2022) Dependence of copper particle size and interface on methanol and CO formation in CO_2 hydrogenation over Cu@ZnO catalysts. Catal Sci Technol 12:551–564
184. Berg R, Prieto G, Korpershoek G et al (2016) Structure sensitivity of Cu and CuZn catalysts relevant to industrial methanol synthesis. Nat Commun 7:13057

185. Nakamura I, Fujitani T, Uchijima T et al (1998) The synthesis of methanol and the reverse water-gas shift reaction over Zn-deposited Cu(100) and Cu(110) surfaces: comparison with Zn/Cu(111). Surf Sci 400:387–400
186. Nakamura I, Fujitani T, Uchijima T et al (1996) A model catalyst for methanol synthesis: Zn-deposited and Zn-free Cu surfaces. J Vac Sci Technol A 14:1464–1468
187. Palomino RM, Ramírez PJ, Liu Z et al (2018) Hydrogenation of CO_2 on ZnO/Cu(100) and ZnO/Cu(111) catalysts: role of copper structure and metal-oxide interface in methanol synthesis. J Phys Chem B 122:794–800
188. Fujitani T, Nakamura I, Watanabe T (1995) Methanol synthesis by the hydrogenation of CO_2 over Zn-deposited Cu(111) and Cu(110) surfaces. Catal Lett 35:297–302
189. Kordus D, Jelic J, Luna ML et al (2023) Shape-dependent CO_2 hydrogenation to methanol over Cu_2O nanocubes supported on ZnO. J Am Chem Soc 145:3016–3030
190. Alayoglu S, Beaumont SK, Zheng F (2011) CO_2 hydrogenation studies on Co and CoPt bimetallic nanoparticles under reaction conditions using TEM, XPS and NEXAFS. Top Catal 54:778–785
191. Pasupulety N, Driss H, Alhamed YA et al (2015) Studies on Au/Cu-Zn-Al catalyst for methanol synthesis from CO_2. Appl Catal A: Gen 504:308
192. Studt F, Sharafutdinov I, Abild-Pedersen F et al (2014) Discovery of a Ni-Ga catalyst for carbon dioxide reduction to methanol. Nat Chem 6:320–324
193. Toyir J, Ramírez de la Piscina P, Fierro JLG et al (2001) Catalytic performance for CO_2 conversion to methanol of gallium-promoted copper-based catalysts: influence of metallic precursors. Appl Catal B: Environ 34:255–266
194. Melian-Cabrera I, Granados ML, Fierro JLG (2002) Reverse topotactic transformation of a Cu–Zn–Al catalyst during wet Pd impregnation: relevance for the performance in methanol synthesis from CO_2/H_2 mixtures. J Catal 210:273–284
195. Melian-Cabrera I, Granados ML, Fierro JLG (2002) Pd-modified Cu–Zn catalysts for methanol synthesis from CO_2/H_2 mixtures: catalytic structures and performance. J Catal 210:285–294
196. Chen S, Abdel-Mageed AM, Mochizuki C et al (2021) Controlling the o-vacancy formation and performance of Au/ZnO catalysts in CO_2 reduction to methanol by the ZnO particle size. ACS Catal 11:9022–9033
197. Guo XM, Mao DS, Lu GZ et al Glycine-nitrate combustion synthesis of CuO-ZnO-ZrO_2 catalysts for methanol synthesis from CO_2 hydrogenation. J Catal 271:178–185
198. Jung KT, Bell AT (2002) Effects of zirconia phase on the synthesis of methanol over zirconia-supported copper. Catal Lett 80:63–68
199. Samson K, Sliwa M, Socha RP et al (2014) Influence of ZrO_2 structure and copper electronic state on activity of Cu/ZrO_2 catalysts in methanol synthesis from CO_2. ACS Catal 4:3730–3741
200. Witoon T, Chalorngtham J, Dumrongbunditkul P et al (2016) CO_2 hydrogenation to methanol over Cu/ZrO_2 catalysts: effects of zirconia phases. Chem Eng J 293:327–336
201. Yang M, Yu J, Tong X et al (2021) Flame-made Cu/ZrO_2 catalysts with metastable phase and strengthened interactions for CO_2 hydrogenation to methanol. Chem Commun 57:7509–7512
202. Lin L, Wang G, Zhao F (2021) CO_2 hydrogenation to methanol on ZnO/ZrO_2 catalysts: effects of zirconia phase. ChemistrySelect 6:2119–2125
203. Ning W, Wang T, Chen H et al (2017) The effect of Fe_2O_3 crystal phases on CO_2 hydrogenation. PLoS ONE 12:e0182955
204. Lei H, Nie R, Wu G et al (2015) Hydrogenation of CO_2 to CH_3OH over Cu/ZnO catalysts with different ZnO morphology. Fuel 154:161–166
205. Liao F, Huang Y, Ge J et al (2011) Morphology-dependent interactions of ZnO with Cu nanoparticles at the materials interface in selective hydrogenation of CO_2 to CH_3OH. Angew Chem Int Ed 50:2162–2165
206. Ouyang B, Tan W, Liu B (2017) Morphology effect of nanostructure ceria on the Cu/CeO_2 catalysts for synthesis of methanol from CO_2 hydrogenation. Catal Commun 95:36–39
207. Chen H, Cui H, Lv Y et al (2022) CO_2 hydrogenation to methanol over Cu/ZnO/ZrO_2 catalysts: effects of ZnO morphology and oxygen vacancy. Fuel 314:123035
208. Khobragade R, Roškarič M, Žerjav G et al (2021) Exploring the effect of morphology and surface properties of nanoshaped Pd/CeO_2 catalysts on CO_2 hydrogenation to methanol. Appl Catal A: Gen 627:118394
209. Zabilskiy M, Ma K, Beck A et al (2021) Methanol synthesis over Cu/CeO_2-ZrO_2 catalysts: the key role of multiple active components. Catal Sci Technol 11:349–358
210. Zhan H, Li F, Gao P et al (2014) Methanol synthesis from CO_2 hydrogenation over La-M-Cu-Zn-O (M = Y, Ce, Mg, Zr) catalysts derived from perovskite-type precursors. J Power Sources 251:113–121
211. Angelo L, Kobl K, Tejada LMM et al Study of $CuZnMO_x$ oxides (M = Al, Zr, Ce, CeZr) for the catalytic hydrogenation of CO_2 into methanol. C R Chim 18:250–260
212. Liu X-M, Yan Z-F, Lu G-Q (2006) Role of nanosized zirconia on the properties of Cu/Ga_2O_3/ZrO_2 catalysts for methanol synthesis. Chin J Chem 24:172–176
213. Ma Y, Wang J, Goodman KR et al (2020) Reactivity of a zirconia-copper inverse catalyst for CO_2 hydrogenation. J Phys Chem C 124:22158–22172
214. Wang R, Wang H, Weng X et al (2021) Exploring the phase transformation in ZnO/Cu(111) model catalysts in CO_2 hydrogenation. J Energy Chem 60:150–155
215. Wu C, Lin L, Liu J et al (2020) Inverse ZrO_2/Cu as a highly efficient methanol synthesis catalyst from CO_2 hydrogenation. Nat Commun 11:5767
216. Lyu H, Hu B, Liu G et al (2020) Inverse decoration of ZnO on small-sized Cu/SiO_2 with controllable Cu-ZnO Interaction for CO_2 hydrogenation to produce methanol. Acta Phys Chim Sin 36 (X):1911008
217. Zhang C, Wang L, Etim UJ et al (2022) Oxygen vacancies in Cu/TiO_2 boost strong metal-support interaction and CO_2 hydrogenation to methanol. J Catal 413:284–296
218. Shen C, Bao Q, Xue W et al (2022) Synergistic effect of the metal-support interaction and interfacial oxygen vacancy for CO_2 hydrogenation to methanol over Ni/In_2O_3 catalyst: a theoretical study. J Energy Chem 65:623–629
219. Wang W, Qu Z, Song L et al (2020) CO_2 hydrogenation to methanol over Cu/CeO_2 and Cu/ZrO_2 catalysts: tuning methanol selectivity via metal-support interaction. J Energy Chem 40:22–30
220. Zhu J, Ciolca D, Liu L et al (2021) Flame synthesis of Cu/ZnO-CeO_2 catalysts: synergistic metal-support interactions promote CH_3OH selectivity in CO_2 hydrogenation. ACS Catal 11:4880–4892
221. Rui N, Sun K, Shen C et al (2020) Density functional theoretical study of Au_4/In_2O_3 catalyst for CO_2 hydrogenation to methanol: the strong metal-support interaction and its effect. J CO_2 Util 42:101313
222. Zhang L, Liu X, Wang H et al (2021) Size-dependent strong metal-support interaction in Pd/ZnO catalysts for hydrogenation of CO_2 to methanol. Catal Sci Technol 11:4398–4405
223. Chinchen GC, Waugh KC, Whan DA (1986) The activity and state of the copper surface in methanol synthesis catalysts. Appl Catal 25:101–107
224. Pan WX, Cao R, Roberts DL et al (1988) Methanol synthesis activity of Cu/ZnO catalysts. J Catal 114:440–446
225. Burch R, Chappell RJ (1988) Support and additive effects in the synthesis ofmethanol over copper catalysts. Appl Catal 45:131–150
226. Robbins JL, Iglesia E, Kelkar CP et al (1991) Methanol synthesis over Cu/SiO_2 catalysts. Catal Lett 10:1–10
227. Kurtz M, Wilmer H, Genger T et al (2003) Deactivation of supported copper catalysts for methanol synthesis. Catal Lett 86:77–80
228. Fichtl MB et al (2014) Counting of oxygen defects versus metal surface sites in methanol synthesis catalysts by different probe molecules. Angew Chem Int Ed 53:7043–7047
229. Kuld S, Conradsen C, Moses PG et al (2014) Quantification of zinc atoms in a surface alloy on copper in an industrial-type methanol synthesis catalyst. Angew Chem Int Ed 53:5941–5945
230. Wang G-C, Nakamura J (2010) Structure sensitivity for forward and reverse water-gas shift reactions on copper surfaces: a DFT study. J Phys Chem Lett 1:3053–3057
231. Cai Z, Huang M, Dai J et al (2021) Fabrication of Pd/In_2O_3 nanocatalysts derived from MIL-68(In) loaded with molecular

metalloporphyrin (TCPP(Pd)) Toward CO_2 hydrogenation to methanol. ACS Catal 12:709–723
232. Frei MS, Mondelli C, García-Muelas R et al (2021) Nanostructure of nickel-promoted indium oxide catalysts drives selectivity in CO_2 hydrogenation. Nat Commun 12:1960
233. Wang J, Li G, Li Z et al (2017) A highly selective and stable ZnO-ZrO_2 solid solution catalyst for CO_2 hydrogenation to methanol. Sci Adv 3:e1701290
234. Lee K, Anjum U, Araújo TP et al (2022) Atomic Pd-promoted $ZnZrO_x$ solid solution catalyst for CO_2 hydrogenation to methanol. Appl Catal B: Environ 304:120994
235. Lee K, Mendes PCD, Jeon H et al (2023) Engineering nanoscale H supply chain to accelerate methanol synthesis on $ZnZrO_x$. Nat Commun 14:819

Publisher's Note